Muon Identification Certification for p17 data

Thomas Gadfort[a], Gavin Hesketh[b], Vincent Lesne[c], Mark Owen[d], Raimund Ströhmer,[e], Boris Tuchming[f]

for the DØ Muon Algorithm and Identification group.

[a] University of Washington, USA
[b] Northeastern University, USA
[c] Université Blaise Pascal, Clermont-Ferrand, France
[d] University of Manchester, UK
[e] Ludwig-Maximilians-Universität, München, Germany
[f] DAPNIA/SPP, CEA-Saclay, France

Abstract

This note reviews muon identification in p17 data. The definitions of basic objects related to muons are given: muon quality, track quality, muon isolation, trigger objects. Some details on trigger and identification efficiencies along with backgrounds and fake rates are also discussed.

Contents

1 Introduction

Muons in D0 can be identified through three independent detector subsystems. The 3 layer muon detector system with its toroid magnet covers more than 90% of the angular acceptance up to a pseudo-rapidity $|\eta| = 2$. It provides unambigious muon identification with a momentum measurement. A muon identified on the basis of the information provided by the muon detector is called a "local muon".

The central tracking system (consisting of the Silicon Microstrip Tracker – SMT – and the Central Fiber Tracker – CFT) provides accurate momentum resolution and is highly efficient at finding tracks in the whole angular acceptance of the muon detector. A local muon that is successfully matched with a central track is called a "central track-matched muon".

A third independent muon confirmation can be obtained by looking for a MIP signature in the calorimeter. The capability to identify muons using the calorimeter is called "Muon Tracking in the Calorimeter" or "MTC" and is still in development. The current MTC algorithm has a typical efficiency of $\approx 50\%$, far less efficient than the other muon signatures.

This note describes the certified Muon Identification (MuonID) definitions to be used with the p17 data arising from version of the D0 event reconstruction software and passed through the p18 version of d0correct.

The p17 definitions of the muon quality and track quality criteria are explained in sections 3.1 and 3.2. Section 3.3.2 contains some discussion of muon isolation. A brief description of the main muon backgrounds, and cuts that can be used to reduce them, is in section 8. MuonID, tracking and trigger efficiencies are studied in sections 5, 6.1.2 and 7. Finally, momentum resolution is discussed in section 9.

2 Summary: p17 with respect to p14 muons

Here is a brief summary of what the user accustomed to muon analysis in p14 data has to know when analyzing p17 data (with p18 d0correct).

2.1 Improvements at the reconstruction level

- When combining segments in local tracking, the number if hits as well as χ^2 is now taken into account.
- Improved matching of central tracks to BC segments.
- PDT pad information is used to improve ϕ resolution in the central A-layer.
- Muon certification variable now filled by d0reco (e.g. isLoose, isCosmic etc).

2.2 Changes in MuonId

- Same MuonId qualities and types for the muon system.
- For muons matched to central track, three types of central track qualities have been defined (track_tight, track_medium, track_loose).
- In the case of track matched muons, the default muon kinematics now come directly from the central track rather than a global fit (the central track was found to have better resolution than the global fit).
- In case of track without SMT hits, imposing the central tracks to arise from the reconstructed primary vertex improves the momentum resolution.
- The muon momentum smearing for Monte-Carlo is run by default.
- The Cosmic Veto (IsCosmic()) now considers separatly the B and the C scintillator time whereas we were cutting on the average in p14.
- number of minor bug fixes and updates.

2.3 Muon quantities in the data

The reader is invited to refer to [2] for more details.

- The central track matching χ^2 is now divided by the number of degrees of freedom. Analyzers cutting on the χ^2 have to change their selection cut by dividing the p14 threshold by the number of degrees of freedom, 3 or 4 (variable *ndof* is available in CAF and TMB).
- Some unused variables have been removed from the TMB.
- B and C layer scintillator times are now available separately.
- Availability of expanded error words.

- The p17 thumbnail (or TMB++) also stores the muon hit chunks - the PDTHitChunk, MDTHitChunk and MSCHitChunk, as well as the central tracker hit chunks and calorimeter cells. In principle, this makes it possible to re-run the muon reconstruction from the TMB++. However this re-running of the reconstruction from TMB++ is not working yet.

2.4 CAF features

The implementation of muons objects in the Common Analysis Format [6] make analysis easier:

- Three types of TMBMuons have been defined and are stored in the TMBMuon branch [3]: Local muon, Central Muon, Smeared MC muon. The user have the choice to:
  - Use the default TMBMuon variables which provide the best possible information, depending upon the context (eg: p_T central for a track matched muon, smeared p_T for MC, or p_T local for unmatched muon).
  - Decide exactly with which type of muon he wants to work.
- The possibility to run the Muon Smearing procedure within CAF analysis as of release p18.06 [8].
- Presence of Muon Selector with standard definition of muon cuts [9].
- Possibility to correct for DATA/MC difference regarding efficiencies [10]
  - For muonid efficiency
  - For tracking efficiency
  - For isolation efficiency

  These corrections are actually valid only for high p_T muons ($p_T > 15$ GeV).
- Possibility to modelize trigger efficiency[10, 11]. These efficiencies are actually valid only for high p_T muons ($p_T > 15$ GeV).

3 Object definitions

3.1 The p17 muon quality definitions

Reconstructed muon candidates are classified using two parameters: muon *type* and muon *quality*. The *type* of muon is given by the parameter *nseg*. A positive value of *nseg* indicates that the muon reconstructed in the muon system ("local muon") was matched to a track in the central tracking system. A negative value of *nseg* tells that the local muon could not be matched to a central track. The absolute value $|nseg| = 1$, 2, or 3 respectively indicates that the local muon is made up of A-layer only hits, B or C-layer only hits (outside the toroid), or both A- and B- or C-layers hits. The different muon types with their respective values of *nseg* are listed in Table 1. Additional information about the various muon types can be found in [2].

nseg	**Muon Type**	**Central track matching algorithm**	**MTC matching criterion**
3	Central track + local muon track (A and BC layer)	Muon to central if local muon track fit converged. Central to muon otherwise	$\Delta\eta$, $\Delta\phi$ between MTC and central track extrapolated to calorimeter
2	Central track + BC only	central to muon	as above
1	Central track + A only	central to muon	as above
0	Central track + muon hit or central track + MTC	central to muon central to calorimeter	as above
-1	A segment only	no match	$\Delta\eta$, $\Delta\phi$ between MTC and and A-layer segment
-2	BC segment only	no match	$\Delta\eta$, $\Delta\phi$ between MTC and and BC-layer segment
-3	local muon track (A + BC)	no match	$\Delta\eta$, $\Delta\phi$ between MTC and local muon track at A-layer if fit converged or else A-segment position

Table 1: *Overview of the different muon types.*

The classification according to muon type, and the underlying muon reconstruction algorithm did not change with respect to p14. The second parameter used to classify muons is the *quality*. The muon quality can be "Loose", "Medium" or "Tight". The Tight definition has remained unchanged since p10. The Medium and Loose efficiencies were optimized by loosening the

requirements on the local muon in regions with reduced acceptance and by instead requiring in these regions a confirmation from the central tracking system. The resulting p17 Loose and Medium criteria are optimised for efficiency and less sensitive to the detailed geometry of the muon detector. However, in the case of non-isolated muons, there are indications that medium and loose muons suffer from higher background / fake rates. This is discussed in section 8.3. The definitions for Tight, Medium and Loose are given below. Detailed information about the p17 Muon Id software and object definitions can be found on the Muon Id web page [1].

- **Tight muons**
  This definition has not changed since p10. Only $|nseg| = 3$ muons can be Tight. A muon is Tight if it has:
  - at least two A layer wire hits
  - at least one A layer scintillator hit
  - at least three BC layer wire hits
  - at least one BC scintillator hit
  - a converged local fit ($\chi^2_{\rm loc}$ >0)
- **$|nseg|$=3 Medium/Loose muons**
  When an $|nseg|$=3 muon candidate fails the Tight criteria it might still be Medium or Loose. An $|nseg| = 3$ muon is Medium if it has:
  - at least two A layer wire hits
  - at least one A layer scintillator hit
  - at least two BC layer wire hits
  - at least one BC scintillator hit (except for central muons with less than four BC wire hits).

  An $|nseg| = 3$ Loose muon is defined as a Medium muon but allowing one of the above tests to fail, with the A wire and scintillator requirement treated as one test and requiring always at least one scintillator.
- **$nseg$=+2 Loose/Medium muons**
  Muons with $|nseg| < 3$ can only be Loose or Medium if they are matched to a central track. $nseg$=2 muons are muons with a BC segment matched with a central track. Loose requires:
  - at least one BC layer scintillator hit
  - at least two BC layer wire hits

  An $nseg$=2 muon is defined as Medium if it fullfills the above requirements and if it is located in the bottom part of the detector (octant 5 and 6 with $|\eta^{detector}|$ <1.6).
- **$nseg$=+1 Loose/Medium muons**
  Muons with $nseg$=1 are muons with an A segment matched with a central track. An $nseg$=1 muon is Loose if it has:

– at least one scintillator hit

– at least two A layer wire hits.

An *nseg*=1 muon is defined as Medium if it fullfills the above requirements and if it is located in the bottom part of the detector (octant 5 and 6 with $|\eta^{detector}|$ <1.6). Low momentum *nseg*=1 muons are also defined as Medium. A *nseg*=1 muon is qualified as low momentum muon if its probability to reach the BC layer is less than 0.7 (this can be adjusted by RCP parameter in `muonid/rcp/MuonCandidate.rcp`). The probability maps as a function of the muon momentum and $|\eta|$ are also set by RCP. Figure 1 shows the probability curves (markers) computed with Geant for generated muons with 3<p<4 GeV, 4<p<5 GeV and 5<p<6 GeV.

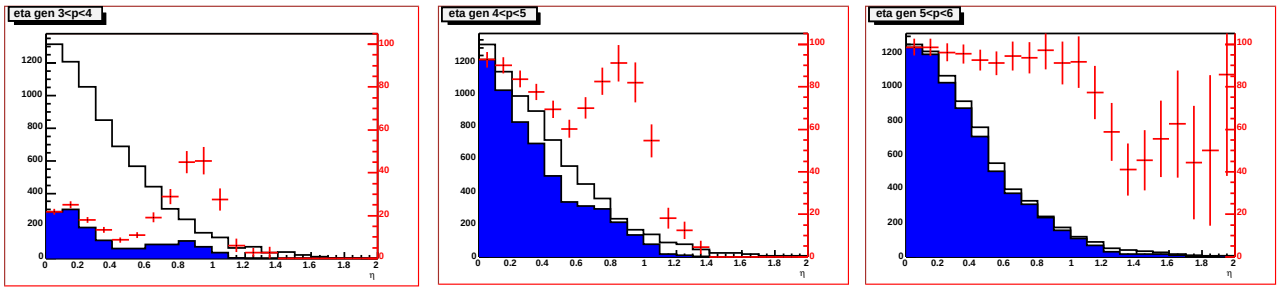

Figure 1: The fraction of muons reaching the BC layer as a function of η (markers), determined from GEANT simulation, for different bins of generated momentum: 3<p<4 (left), 4<p<5 (middle) and 5<p<6 GeV (right). The open (shaded) histograms show the η distribution of the generated muons before (after) reaching the BC layer.

3.2 The p17 tracking quality definitions

To control the purity of muons matched to central track, three qualities of track have been defined. They rely on the following track characteristics:

- number of hits either in the SMT or CFT system.
- χ^2 per degrees of freedom of the central track fit.
- distance of closest approach (in (x,y)) with respect to the primary vertex of the event.

The p17 track quality definitions are the following:

- **loose track**
  A track is loose if $|dca| < 0.2$ cm. If the track has SMT hit the cut is tighten to $|dca| < 0.02$ cm. Note that, for muons from Z decays, the typical resolution observed in the data are 20 μm and 500 μm for respectively tracks with and without SMT hits.

- **medium track**
  A track is medium if it fulfills the loose requirements and if the χ^2 per degrees of freedom is smaller than 4: $\chi^2/\text{d.o.f.} < 4$

- **tight track**
  A track is tight if it fulfills the medium requirements and if it has SMT hits.

3.3 Muon Isolation

3.3.1 Definition of Isolation Variables

Muon isolation cut variables are designed to separate the $W \to \mu\nu$ signal from heavy flavor background ($B \to \mu$). Because muons from heavy flavor decays tend to be embedded inside a jet, these variables are either defined in terms of the tracks near the muon track or calorimeter energy surrounding the muon momentum vector. The five variables used in this section are defined below.

- TrackHalo = $|\sum^{\text{tracks}} p_T|$ in ΔR(track, muon track)< 0.5 cone.
- CalorimeterHalo = $|\sum^{\text{cells}} E_T|$ in $0.1 < \Delta R$(cal-cells, muon cal-track) < 0.4.
- $\Delta R(\mu, jet)$ = Distance to closest jet in $\eta - \phi$ space.
- ScaledCalorimeterHalo = $|\sum^{\text{cells}} E_T/p_T(\mu)|$ in $0.1 < \Delta R$(cal-cells, muon cal-track)< 0.4.
- ScaledTrackHalo = $|\sum^{\text{tracks}} p_T/p_T(\mu)|$ in ΔR(track, muon track)< 0.5 cone.

3.3.2 Definition of Isolation Working Points

Because every analysis has different signal to background requirements, there are many muon isolation working points. These working points are described below

- TopScaledUltraLoose = ScaledTrackHalo < 1.0 and ScaledCalorimeterHalo < 1.0.
- TopScaledVeryLoose = ScaledTrackHalo < 0.5 and ScaledCalorimeterHalo < 0.5.
- TopScaledLoose = ScaledTrackHalo < 0.2 and ScaledCalorimeterHalo < 0.2.
- TopScaledMedium = ScaledTrackHalo < 0.15 and ScaledCalorimeterHalo < 0.15.
- TopScaledTight = ScaledTrackHalo < 0.1 and ScaledCalorimeterHalo < 0.1.
- TopScaledVeryTight = ScaledTrackHalo < 0.05 and ScaledCalorimeterHalo < 0.05.
- TopP14 = ScaledTrackHalo < 0.06, ScaledCalorimeterHalo < 0.08, and ΔR(μ,jet) > 0.5.
- DeltaR = ΔR(μ,jet) > 0.5.
- NPLoose = TrackHalo < 4.0 GeV and CalorimeterHalo < 2.5 GeV.
- NPTight = TrackHalo < 2.5 GeV and CalorimeterHalo < 2.5 GeV.

3.4 Cosmic Veto

The cosmic veto cut is discussed section 8.1. As most of the analyzers are using it, the recommendation of the muon Id group is to veto muons having the loose isCosmic() flag. This veto consists in rejecting cosmic muons using the scintillator hit times (when information is available):

- |A-layer time| < 10 ns
- |B-layer time| < 10 ns
- |C-layer time| < 10 ns

It is worthwhile to notice that the loose medium and tight tracking criteria defined in 3.2 have dca cuts also suppressing cosmic muons.

3.5 Muons with supported CAF DATA/MC corrections

In the next sections the efficiency measurements of muon Id criteria, tracking criteria and isolation criteria are discussed. The trigger efficiencies are also discussed Section 7. These efficiencies are measured for high p_T muons, in order to correct for DATA/MC differences using the muid_eff and caf_eff_utils packages [7, 10]. The trigger object efficiencies are measured to simulate triggers using the caf_trigger package [11].

The efficiency corrections and the trigger efficiencies are valid for only the supported certified muons which are:

- of quality either loose or medium or medium with nseg=3 or tight; and passing the loose cosmic veto, IsCosmic;
- matched to a high p_T ($p_T > 15$ GeV) reconstructed central track of either loose or medium or tight quality;
- not isolated, or isolated according to the working points defined in 3.3.1.

It must be stressed that any departure from these definitions may require new measurements of the offline or trigger efficiencies. It is up to the analyzer to determine to what extent the results stored in the muid_eff package are valid for his own purpose.

The muons object efficiencies are splitted in three terms and stored in the muid_eff cvs package:

1. muonid efficiency $\times$ cosmic veto efficiency $\times$ track matching efficiency
2. tracking efficiency
3. isolation efficiency

4 Cerfication samples

4.1 data sample

For the efficiency computation, the full RunIIa skim 2MUhighpt [5] has been analyzed using the packages wzreco and muo_cert [4]. The efficiency measurements rely on a "tag and probe" method using Z-peak di-muon events. Figure 2 displays some basic quantities of the selected di-muon events: their invariant mass, angular luminosity and run number distributions.

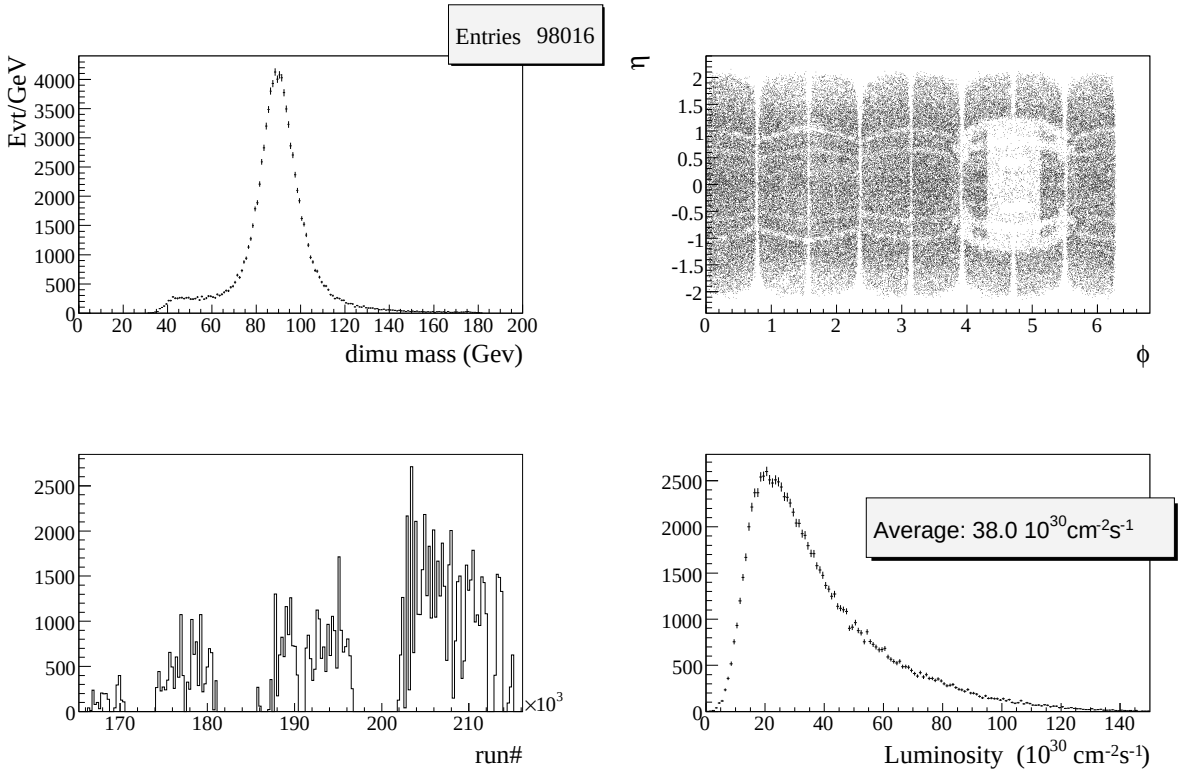

Figure 2: Invariant mass, (η, ϕ) of muons, run number and instantaneous luminosity distributions in events selected for the muon certification.

4.2 MC sample

For the computation of efficiencies with MC and the momentum resolution determination, we used the Pythia $Z \to \mu^+\mu^-$ sample with RequestId 30604. (p17.09.01 MC refixed with p17.09.05).

A package dedicated to duplicate removal was added to *wzreco*. Out of the 225k events of RequestId 30604 65k are kept because they are really independent.

Figure 2 displays some basic quantities of the events selected by *muo_cert*: their invariant mass, angular distributions as well as the luminosity and run number distributions of the zero-bias overlaid events.

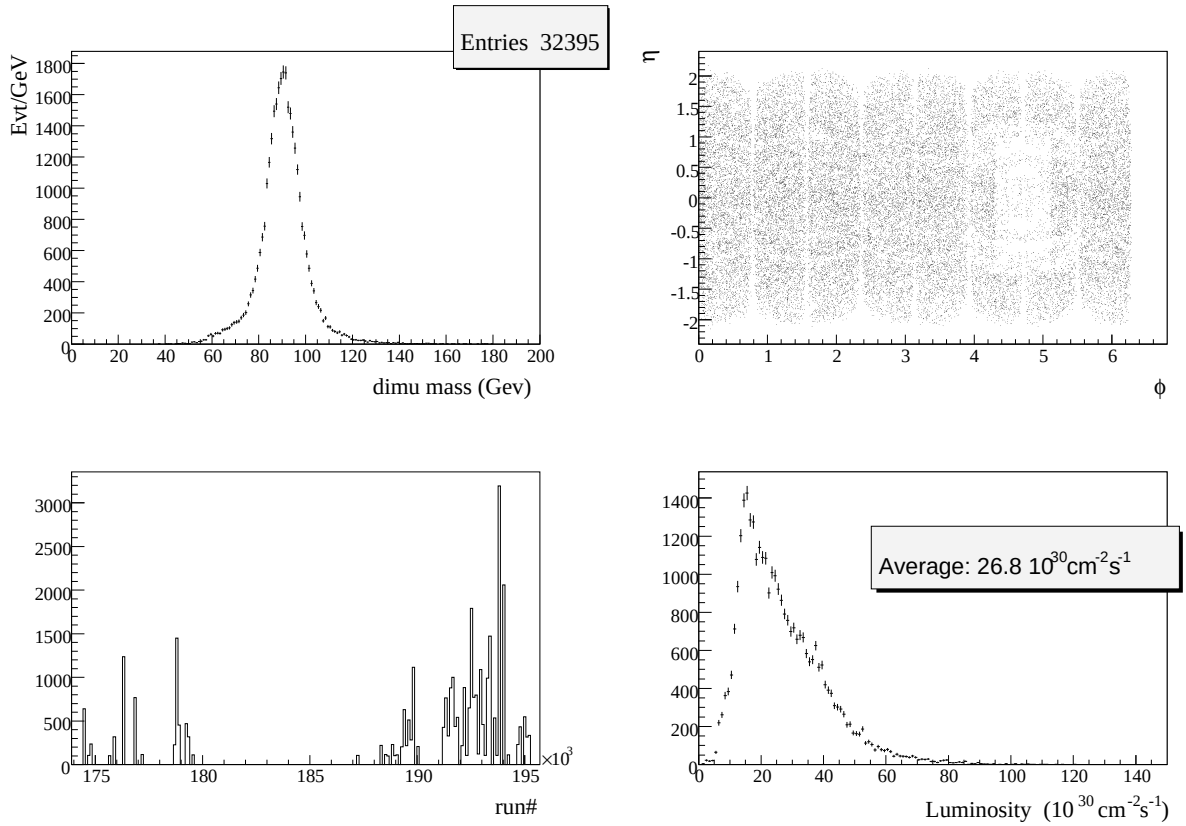

Figure 3: Invariant mass, (η, ϕ) of muons, run number and instantaneous luminosity distributions in MC events for the muon certification.

4.3 Luminosity and number of vertices

For some efficiencies it is worthwhile to study the dependence as a function of luminosity or number of reconstructed vertices. Figure 4 shows the relation between the luminosity and the average number of extra-vertices in the wzreco data sample. Extra vertices means all vertices but the one matched to the $Z \rightarrow \mu^+\mu^-$ production.

No staturation effect is seen on this plot which could arise for example because of saturation in the vertex reconstruction efficiency. On average $\simeq 1$ extra vertex is present on the p17 data sample ($< L > \simeq 40 \times 10^{30}$ cm$^{-2}s^{-1}$). According to this figure the luminosity of $L \simeq 300 \times 10^{30}$ cm$^{-2}s^{-1}$ forseen for Run IIb, corresponds to $\simeq 7$ extra vertices. This relationship may be usefull to extrapolate the efficiency behavior to RunIIb data in the following sections.

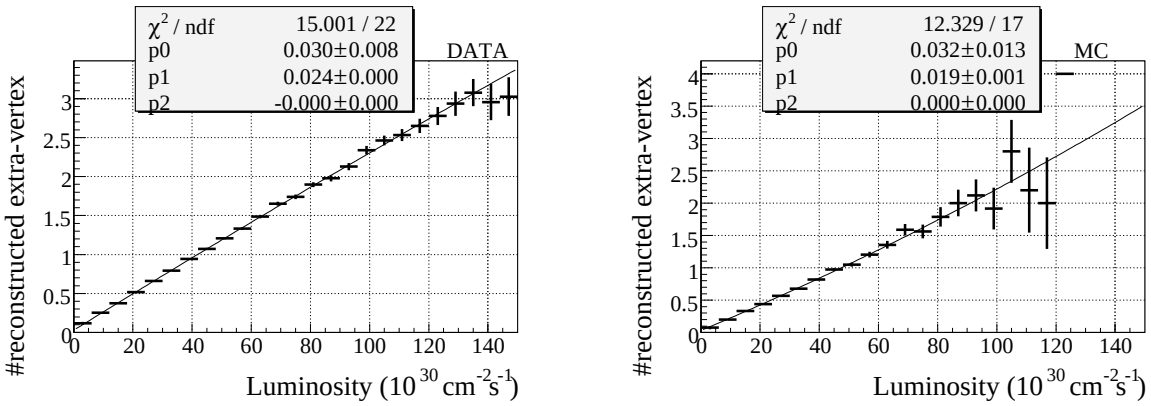

Figure 4: number of extra reconstructed vertices as a function of instantaneous luminosity for both data and MC certification samples. The profile histograms have been fitted with a second degree polynomial.

5 The p17 muon Id efficiency

In this part , the efficiencies for various muon quality criteria are presented. Their dependence in η, φ and the evolution along time are discussed. The quality criteria considered are *loose*, *medium*, *nseg=3 medium* and *tight*.

5.1 Principle of efficiency estimation

The muonid efficiencies are computed using a tag and probe method implemented in the packages `wzreco`/`muo_cert` [4]. $Z \rightarrow \mu^+\mu^-$ events are selected by `wzreco` package using the cuts on the control muon:

- loose muonid quality (using criteria based on the muon system only) ;
- A-layer scintillator $|time| < 7$ ns (B-layer time if no A-scintillator hit);
- matched to a central track of quality *track_medium* (cf section 3.2 page 7);
- $p_T > 30$ GeV/c;
- isolated using cuts $TrackHalo < 3.5$ GeV $CalorimeterHalo < 2.5$ GeV) as defined section 3.3.1;
- fires at least one single muon trigger ;

and the following cuts on the probe:

- track of *track_medium* quality
- $p_T > 20$ GeV
- isolated ($TrackHalo < 3.5$ GeV $CalorimeterHalo < 2.5$ GeV;
- acolinearity between tag and probe ($\pi - |\varphi_1 - \varphi_2| + |\pi - \theta_1 - \theta_2|$) smaller than 0.025;
- $|\Delta z|$ <2cm (between that tag and probe track)

The probe muon, is then matched (either using reconstruction central matching algorithm or the more crude $\Delta R < 0.5$) to muon Id objects to estimate the muon reconstruction efficiency.

5.2 Spatial dependence

The muon reconstruction efficiencies for various muon Id criteria are presented in the (η,φ) plane in Figures 5 and 6, in the latter the muons in the hole region are excluded. The hole region corresponds to the non instrumented bottom part of the muon central detector ($|\eta| < 1.25$ and $4.25 < \varphi < 5.15$). We notice a reduced efficiency in φ close to the octant boundaries and in η in the transition from central to forward regions ($0.5 < |\eta| < 1$). Because of problems in the muon system in the run range 194000-200000, a reduced efficiency is observed in the region ($-1 < \eta < -0.5, \varphi \simeq 3$).

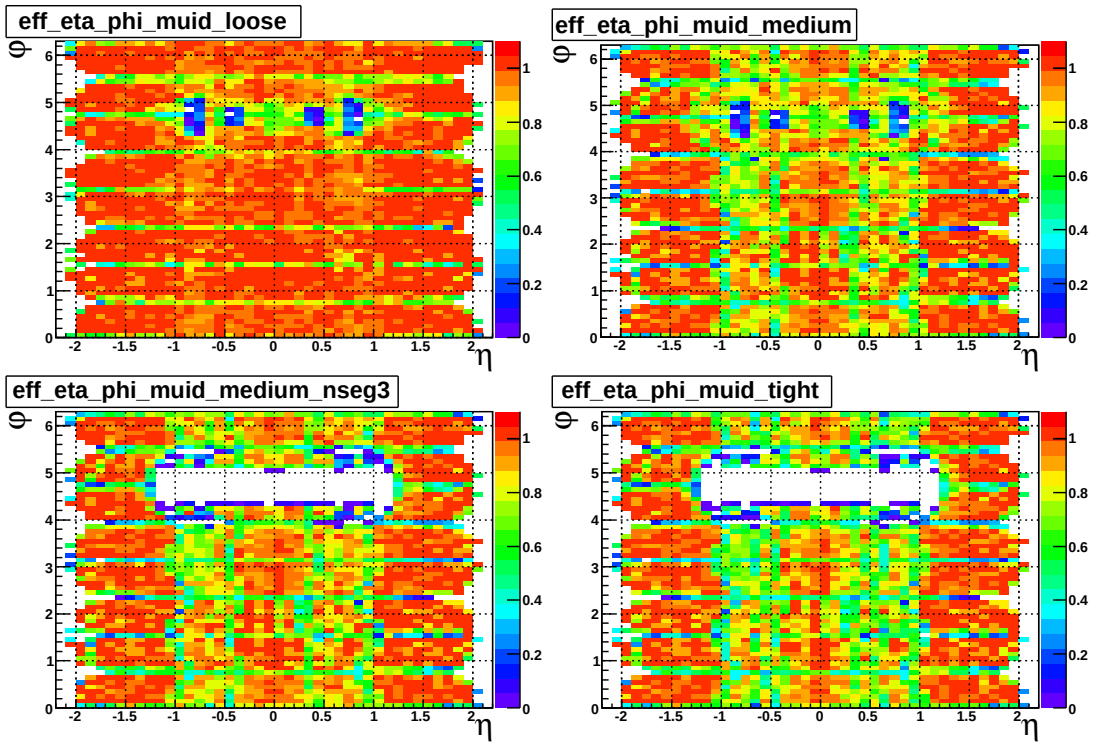

Figure 5: Reconstruction efficiencies in the $\eta - \varphi$ plane for various muon Id criteria.

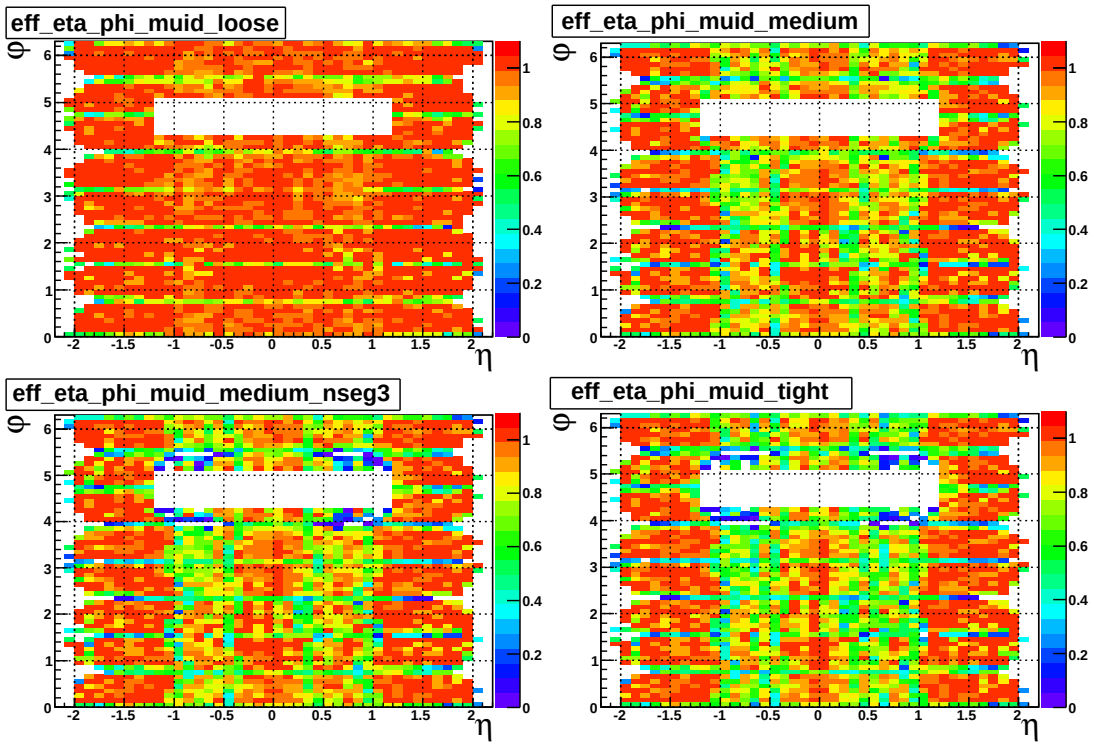

Figure 6: Reconstruction efficiencies in the $\eta - \varphi$ plane for various muon Id criteria. Muons in the hole region are excluded.

5.3 Time dependence

The evolution of the reconstruction efficiencies in function of time is presented in Figure 7. We can distinguish two time periods. Since run number close to 198000 (october 2004), the muon Id efficiency has been increased by 0.5% for loose quality and by 1.5% for the three other criteria. The improvement is supposed to come from modifications made on scintillator system. The effects are more important for the medium, nseg=3 medium amd tight criteria because scintillator hits are required for these muon criteria. The average efficiencies over the full data set are respectivly 94.8%, 83.4%, 80.2% and 75.9% for the loose, medium, nseg=3 medium and tight criteria.

5.4 Instantaneous luminosity dependence

The variation of the muonid efficiencies for the criteria (loose), (medium relative to loose), (tight relative to medium) is shown in Figure 8. The dependence upon the number of exta-vertices (different from the $Z \rightarrow \mu^+\mu^-$ vertex) is also displayed. The luminosity plots shows a very weak improvments that can be attributed to the improvments on the scintillator system. The nvertex plots shows a very weak decreases, less than -1% for nvert=7 (Note that the a luminosity of $300 \times 10^{30} \mathrm{cm}^{-2}\mathrm{s}^{-1}$ would yield an average number of reconstructed vertex of 6-7).

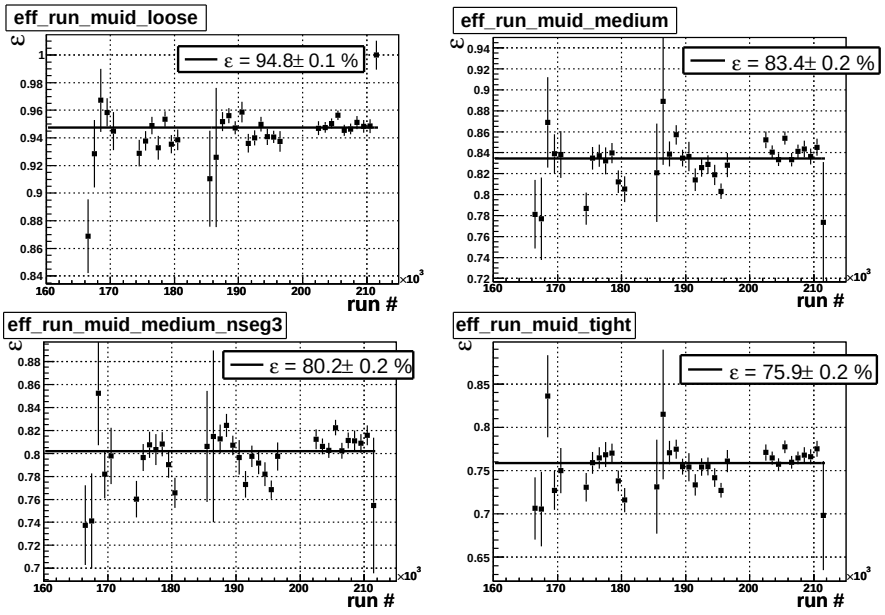

Figure 7: Time evolution of the muon reconstruction efficiency for the different muon Id criteria. Muons in the hole region are not considered.

In conclusion, the muonid criteria are quite unsensitive to the high luminosity of the Tevatron.

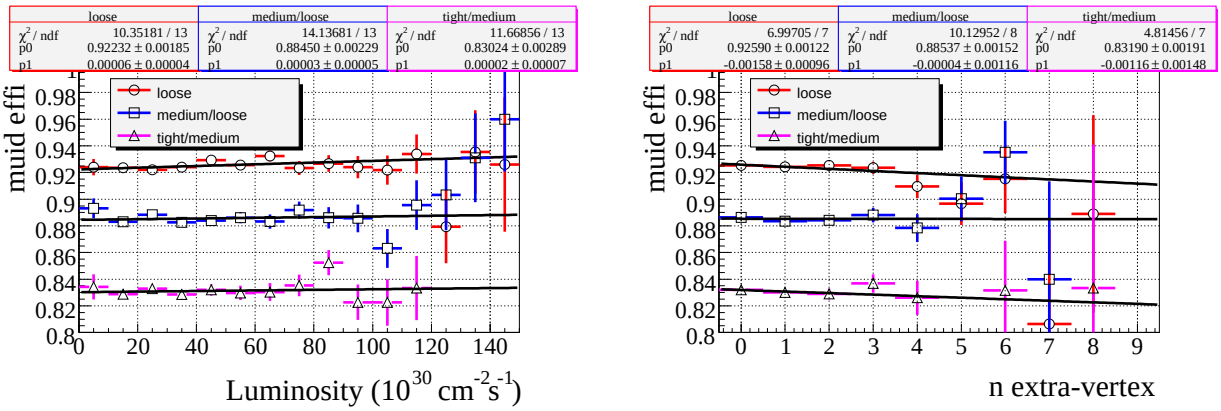

Figure 8: Dependence of the muonid efficiencies with respect to the instantaneous luminosity and the number of extra-vertices. The efficiency has been computed for (loose), (medium relative to loose) and (tight relative to medium).

5.5 DATA/MC muon Id correction

The muonid reconstruction efficiencies of simulated and real muons are different. This can bee seen in Figure 9 where the $\varepsilon(DATA)/\varepsilon(MC)$ ratios as a function of detector η are shown.

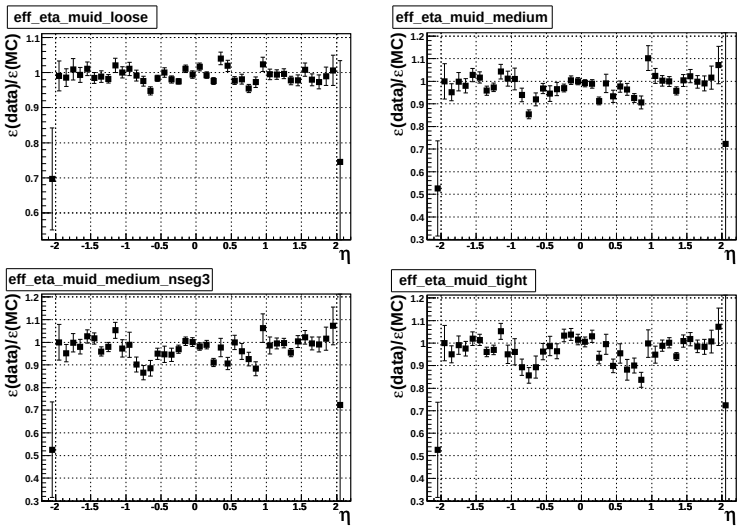

Figure 9: Ratios of data and MC efficiencies for the different muon Id criteria. Muons in the hole region are not considered.

The muonid times central track matching[1] times cosmic veto efficiencies are computed in 2-dimension, as a function of detector η and φ by the package muid_eff [7] for both data and MC. The binning is:
- in φ, 32 bins from 0 to 2π,
- in η 44 bins from -4.2 to 4.2.
The ratio of efficiencies, DATA/MC, has to be applied using the caf_eff_utils package [10] to the simulated muons to correct for the innacuracy of the MC.

Typically, the average correction factors are respectively 0.995, 0.98, 0.97 and 0.97 for respectively the loose, medium, medium nseg3 and tight criteria.

Note that the analyzer has also to further correct for the tracking efficiency, depending on the track quality requirements as described in section 6.3.3.

5.6 Systematic uncertainty on the muon Id efficiency corrections

Several sources of uncertainty may affect efficiency measurements and data/MC correction factors. We try to here to assess them quantitatively. For some specific reason, the reader may find that these numbers can not be applied straightforwardly to his analysis. So this part can also be viewed as a guideline.

[1]Track matching efficiency is the efficiency that a muon reconstructed in the muon system and the corresponding reconstructed central track are matched together. Typically it is of the order of 99%

5.6.1 Generality on the tag and probe method

The tag and probe method consists actually in measuring

$$\varepsilon_{tag\&probe} = \frac{< \varepsilon_{tag} \times \varepsilon_{probe-presel} \times \varepsilon_{test} >}{< \varepsilon_{tag} \times \varepsilon_{probe-presel} >}, \quad (1)$$

where ε_{tag} is the selection efficiency of the control muon, $\varepsilon_{probe-presel}$ is the pre-selection efficiency of the test muon, ε_{test} is the efficieny that one wants to measure, and <> means average over run number, luminosity profile, z of primary vertex, phase space distribution ...

In general the analyzer would like to determine $< \varepsilon_{test} >$. Because of correlation between the tag and the probe muon, or because of correlations between the pre-selection of the probe and the criteria to be tested, this quantiy may be different from $\varepsilon_{tag\&probe}$.

It is worthwhile to notice that the relative difference between $\varepsilon_{tag\&probe}$ and $< \varepsilon_{test} >$ is of second order, since it requires that both the efficiencies vary and that they are correlated.

5.6.2 tag and probe bias using MC

A first way to measure a possible bias consists in assessing the difference between the tag and probe measurements and the genuine efficiency in MC events. This has not be done for p17, however results quoted here [13] (p14-pass1) indicate the relative bias amounts to 0.2% for the medium efficiency.

At the first order, such bias is expected to be the same in MC and data and should cancel in the ratio. It is not totally true, since trigger requirements are applied on the data but not on the MC. It is also worthwhile to notice that some changes in wzreco [4] cuts have been made since reference [13] was written.

For both aforementionned reasons, we quote conservatively a 0.2% systematic uncertainty on the ratio of efficiencies.

5.6.3 background contamination

Presence of background in the data may bias downward the efficiency. Possible background may be for example QCD (tag=muon in jets, probe=track from jets), $W \to \mu\nu$ (tag=high p_T muon, probe=track from jets), $Z \to \tau^+\tau^-$ (tag=high p_T muon, probe=charged pion) or cosmic (tag=in time cosmic muon, probe=out of time cosmic muon).

To assess background effect we vary some cuts, that are supposed to change the contamination in background events. The resulting variation may also be due to the tag and probe biases. Thus we also determine the effect of the cut variation in MC events to correct for it.

1. Restricting the measurements to $|m_{\mu\mu} - 91.2| < 15$ GeV yields a relative variation of -0.005% (0.02%) for the loose (medium) efficiency.

2. Constraining the tag and probe to be back to back ($\Delta\varphi > 2.9$) yields a relative variation of 0.4% (0.6%) for the loose (medium) efficiency. A smaller variation is observed in the MC: 0.2% for both loose and medium efficiencies, so that we retains finally $0.4\% - 0.2\% = 0.2\%$ ($0.6\% - 0.2\% = 0.4\%$) as a possible background contamination.

   Note that if we are contaminated by $W \to \mu\nu$ events, this cut is supposed to suppres them.

3. Constraining the events to have no reconstructed jet, an increase of 0.3% (0.4%) for the loose (medium) efficiency is observed while in the MC the increase is 0.1% (0.01%) for the loose (medium) efficiency. Because of the MC results, we retain 0.2% (0.4%) as a possible background contamination

   Note that if we are contaminated by QCD events, this cut is supposed to reduce them.

4. Tightening the dca cut to 0.1 cm, no sizeable variation is observed.

This series of results demonstrate that the contamination in background is small. The fact that the variations are twice larger for the medium case is somewhat contradictory with the hypothesis that these variations are entirely due to background contamination. But we still quote them as systematic uncertainties

For the mediumnseg3 and tight case we do observe similar variation as for the medium efficiency. So summing quadraticaly the observed variations, we finally quote 0.3% uncertainty for the loose DATA/MC correction and 0.6% for the medium, medium nseg3, and tight correction.

5.6.4 Time and luminosity

As observed in section 5.3 and 5.4, the variation as a function of time and luminosity are at the level of 1.5%. The possible bias yielded if a given selection is performed on a different sample that the one used for certification is negligible.

This can be easily understood with the following extreme example: one analyzes 50% of the run prior 200000 and 100% of the run after 200000. Then the efficiency given by muonid do not match the efficiency needed by the analysis at the level of less than $\simeq 0.3\%$.

So no systematic is quoted for possible time and luminosity variation.

5.6.5 Choice of binning

The efficiency corrections are parameterized in a binned 2d map, as described Section 5.5 By doubling or halfing the size of the binning in both the η and φ directions and convoluting with the proper η φ muon distribution, a 0.15% increase is observed for the muon tight efficiency. The variation amounts to 0.1% for the medium efficiency and is negligible for the loose muon efficiency.

5.6.6 limited statistics

The limited size of both MC and data samples yields a stastical uncertainty for the data/MC correction. It amounts to 0.1%, 0.2% and 0.3% for respectively the loose medium and tight tracking criteria.

5.6.7 Summary

In Table 2, the figures about systematic uncertainties regarding the muon Id correction factors are summarized. As the CAF correction utilities already accounts for the statistical uncertainties, it is not added to the total.

Source of systematic	loose	medium	medium nseg=3	tight
tag and probe bias	0.2%	0.2%	0.2%	0.2%
background and cut variations	0.3%	0.6%	0.6%	0.6%
luminosity and time	-	-	-	
finite binning	0.1 %	0.15%	0.15%	0.15 %
data and MC stat	0.2 %	0.2%	0.2%	0.2%
Total w/o stat	0.4%	0.7 %	0.7 %	0.7%

Table 2: Summary of systematic uncertainties on muon Id correction factors

5.7 Efficiency correction and systematic summary for Muon Id

In Table 5, the typical average numbers are given. They may depend upon the topology and η φ distribution of the muons, so these are only indicative results:

Muon type	loose	medium	medium nseg=3	tight
Efficiency in data	94.8%	83.4%	80.2%	75.9%
DATA/MC correction	0.995 ± 0.004	0.98 ± 0.007	0.97 ± 0.007	0.97 ± 0.007

Table 3: Figures for MuonId efficiencies, correction factor and systematics

6 The p17 tracking and SMT hit efficiencies

In this part, the efficiencies of tracking for various track quality criteria are presented. The tracking efficiency includes the CFT efficiency and the matching efficiency between local muons and central tracks. The SMT hit efficiency, corresponding to the probability for a central track to have reconstructed hits in the SMT detector, is also considered. Their dependence in η, z, time and luminosity are discussed.

6.1 Principle of efficiency estimation

6.1.1 SMT hit efficiency

The SMT hit efficiency is obtained by measuring the fraction of muon tracks with SMT hits after the $Z \rightarrow \mu^+\mu^-$ selection described in [12]. To remove trigger bias, the events must have fired a dimuon trigger (with no track trigger requirement).

6.1.2 Tracking efficiency

The tracking efficiencies are computed using a tag and probe method implemented in the packages `wzreco/muo_cert` [4]. $Z \rightarrow \mu^+\mu^-$ events are selected by `wzreco` package using the cuts on the control muon:

- loose muonid quality (using criteria based on the muon system only) ;
- matched to a central track
- $p_T > 30$ GeV/c;
- $dca < 200$ μm (where dca is relative to beam position); given their dca resolution ($\simeq$ 500 μm) this cut actually tends to remove tracks without SMT hit;
- isolation using cuts $TrackHalo < 3.5$ GeV $CalorimeterHalo < 2.5$ GeV) as defined section 3.3.1;

and the following cuts on the probe:

- loose muonid quality (using criteria based on the muon system only) ;
- $p_{Tloc} > 15$ GeV, where p_{Tloc} is measured in the muon system
- $\Delta R > 2$ between the tag and probe
- $\Delta t < 6$ ns, where Δt is the difference of time between the tag and the probe muon (given by the scintillators, either A-layer or B-layer)

To remove trigger bias, the events must have fired a dimuon trigger (with no track trigger requirement).

6.2 SMT hit efficiency

6.2.1 Spatial dependence

The SMT hit efficiency versus pseudorapidity is presented in Figure 10. The small efficiency observed in the central region is explained by the geometry of the SMT detector. Indeed, it is not designed to detect charged particles with a path transverse to its surface (i.e along (x,y) plane) such as particles with small $|\eta|$.

Because of the detector geometry, the SMT hit efficiency is highly dependent on the z position of the charged track as illustrated in Figure 11. The high correlation between η and z is also shown in Figure 11. The (φ, η) efficiency map is also shown in Figure 11. This plot demonstrates that some regions of the SMT are highly innefficient because of dead or buggy HDI's. An inneficiency map has been implemented in the MC, but it does not match the pattern from the data as can be observed if we compared Figure 10 and Figure 11.

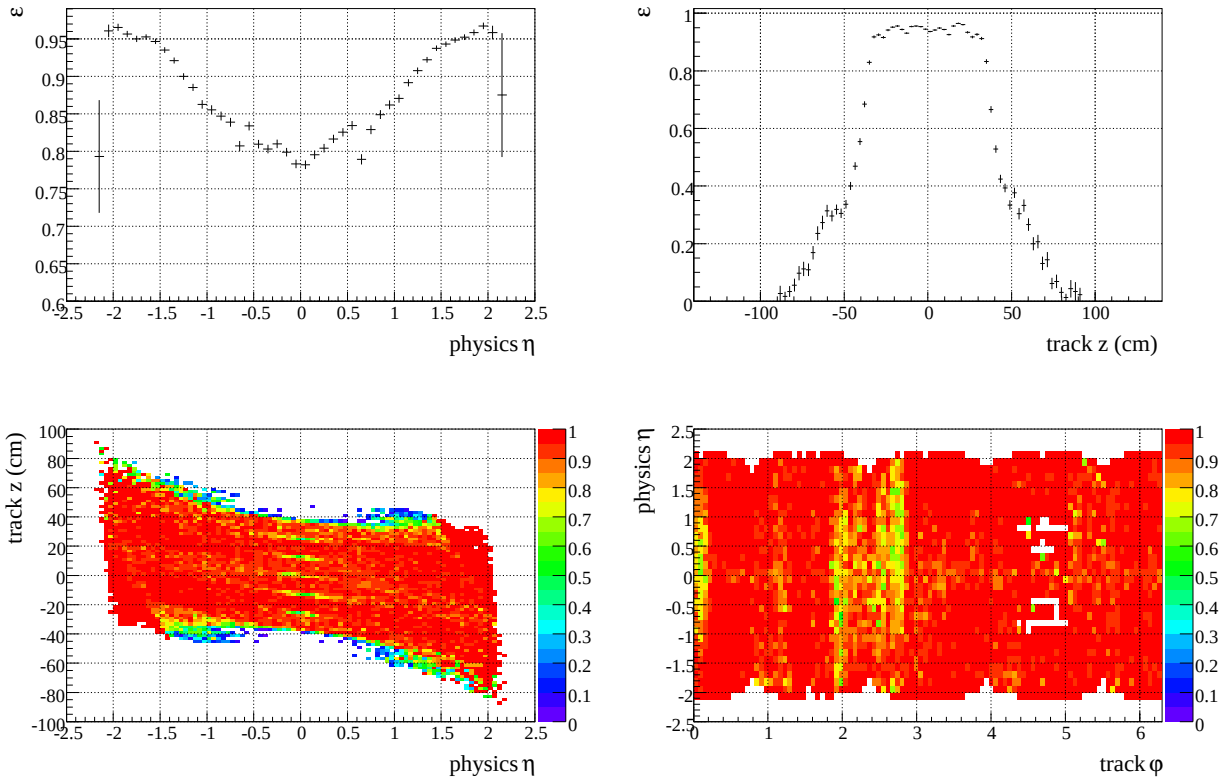

Figure 10: SMT hit efficiency in data events as a function of η, φ and z at dca of the muon track. z at dca of the muon track. The (φ, η) plot is obtaind with the cut $|z| < 20$ cm.

6.2.2 Time dependence

The evolution of the SMT hit efficiency along time is presented in Figure 12. The average efficiencies over the full data set is 88.8%. A 4% improvement in the SMT efficiency is observed

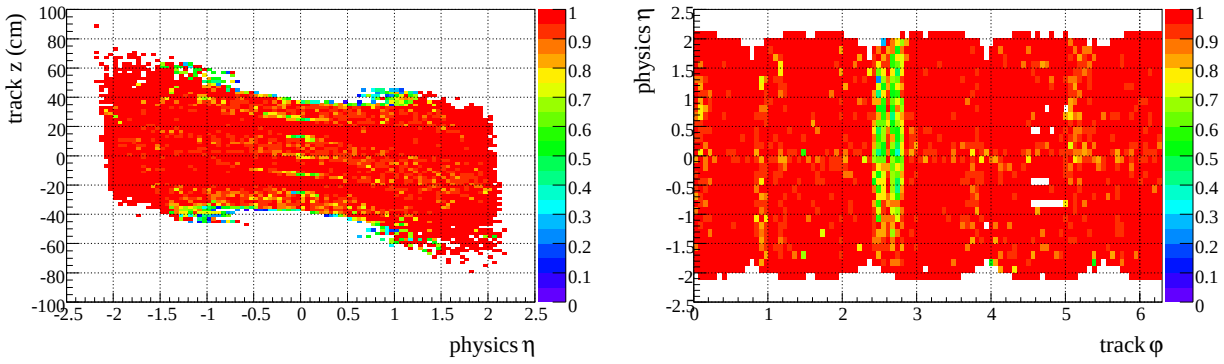

Figure 11: SMT hit efficiency in MC events as a function of η, φ and z at dca of the muon track. The (φ, η) plot is obtaind with the cut $|z| < 20$ cm.

after run number 195000.

One of the cause of the increased efficiency is found to be the change of the beam geometry. Indeed, the beam is sharper in z since this time period as shown in Figure 13, while the SMT hit efficiency depends highly upon the z of the track. The question of beam shape modelling in MC is further discussed in section 6.4.6.

Another cause is found by looking at the efficiency as a function of z for two run periods in Figure 13. On average the efficiency is increased by $\simeq 1\%$ for run > 195000. This is explained by the improved SMT firmware and the recovery of a few bad HDI's.

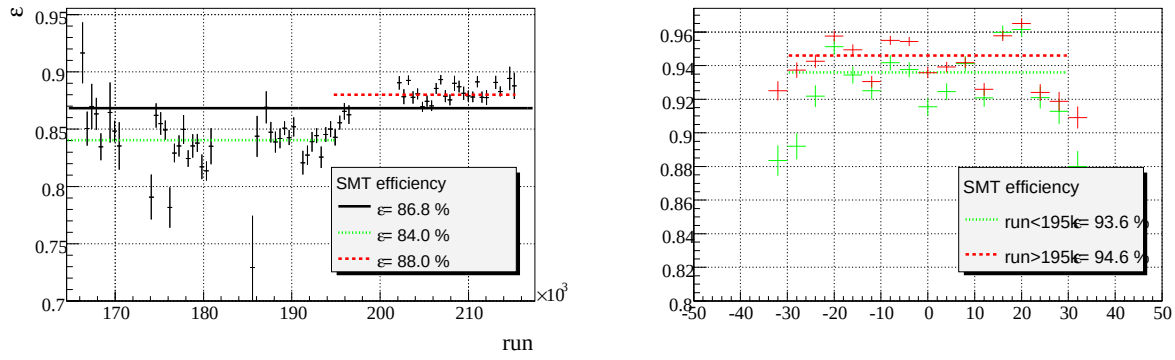

Figure 12: Time evolution of the SMT hit efficiency. On the right, efficiency as a function of z for two time periods.

6.2.3 Luminosity dependence

The beam shape depends on the instantaneous luminosity. The beam is sharp in z at the beginning of a store i.e at high luminosity and widen with decreasing luminosity. The SMT hit

efficiency is then luminosity dependent as illustrated in Figure 13. A 8% variation is observed in SMT hit efficiency when considering the full data set. It is reduced to two times 4% when splitting the data set in two run ranges, before and after run 195000.

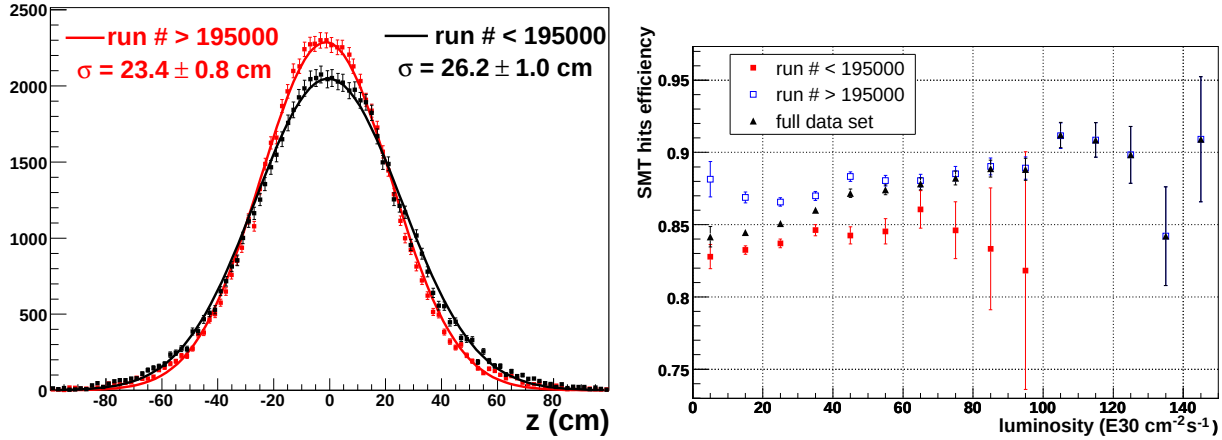

Figure 13: On the left, z of the muons as observed in the wzreco sample, for run number $<$ 195000 (black) and run $>$ 195000 (red). According to a gaussian fit, the average beam width along z is reduced by 10% since run 195000. On the right, SMT hit efficiency as a function of instantaneous luminosity in the full data set (black triangles), for run $<$ 195000 (red squares) and run $>$ 195000 (blue empty squares).

6.2.4 DATA/MC ratio

The $\varepsilon(DATA)/\varepsilon(MC)$ ratio for the SMT hit efficiencies is presented in Figure 14.

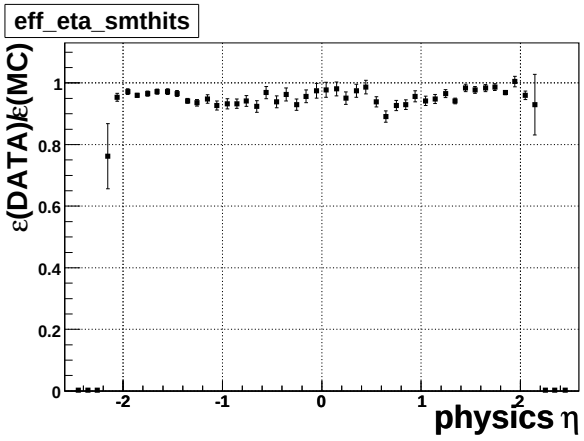

Figure 14: Ratio of data and MC SMT hit efficiencies as a function of pseudorapidity.

6.3 Tracking efficiency

6.3.1 Spatial dependence

The track reconstruction efficiencies for various track qualities are presented as a function of pseudorapidity in Figure 15.

The inefficiency observed in the central region ($|\eta| < 1$) is related to the SMT hit inefficiency observed in section 6.2.1. The tracking efficiency depends on the z position of the muon. This dependence is presented in Figure 16.

On average the tracking efficiencies are 94.2%, 91.0%, and 81.5% for respectiveley the loose, medium and tight tracking criteria.

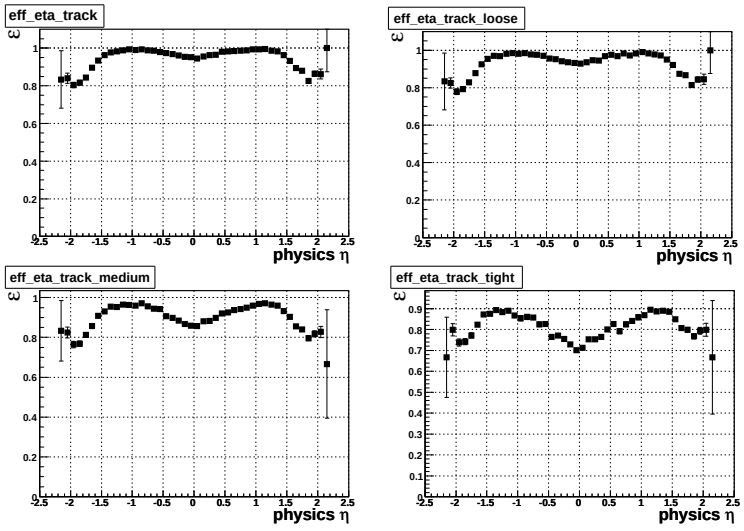

Figure 15: Tracking efficiencies as a function of pseudorapidity for various track qualities.

The tracking efficiency is then estimated for 5 bins of z. The results are presented for various quality criteria in Figures 17, 18, 19 and 20.

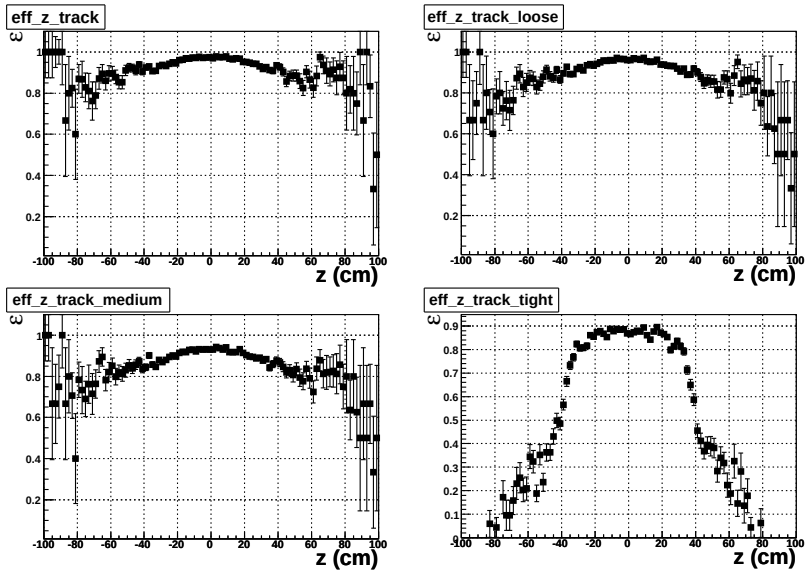

Figure 16: Tracking efficiencies as a function of z position of the muon for various track qualities.

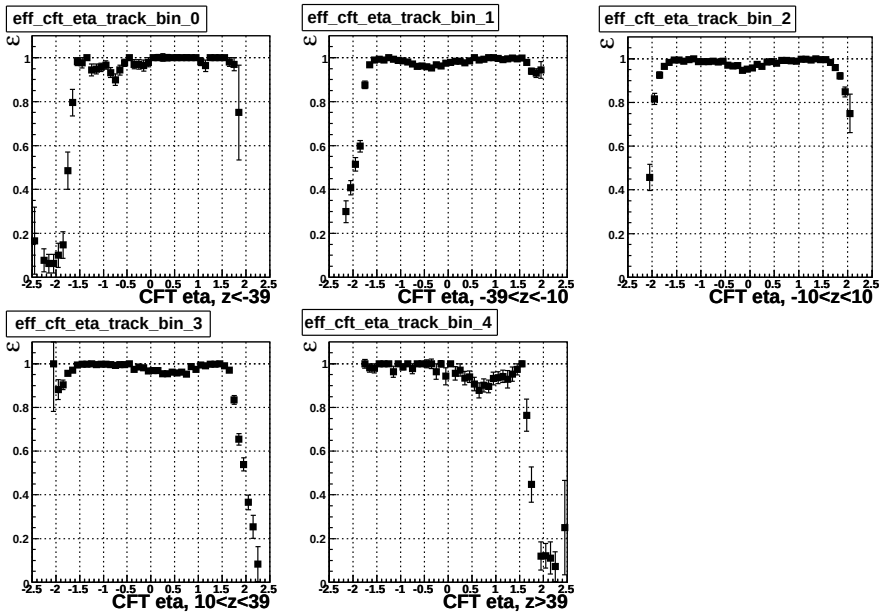

Figure 17: Tracking efficiency as a function of the reconstructed z position at dca of the muon. No quality is required for the track

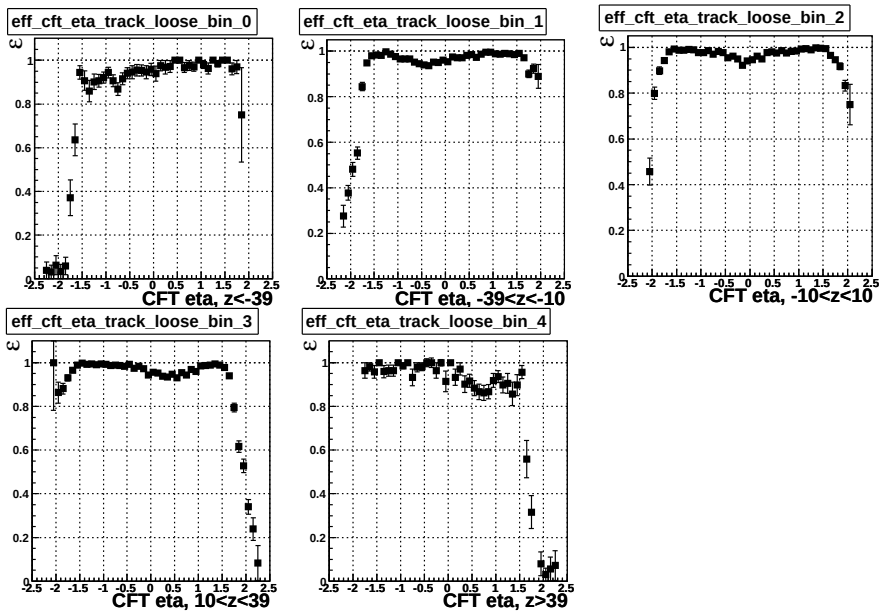

Figure 18: Tracking efficiency as a function of the reconstructed z position at dca of the muon. Only loose or better tracks are considered.

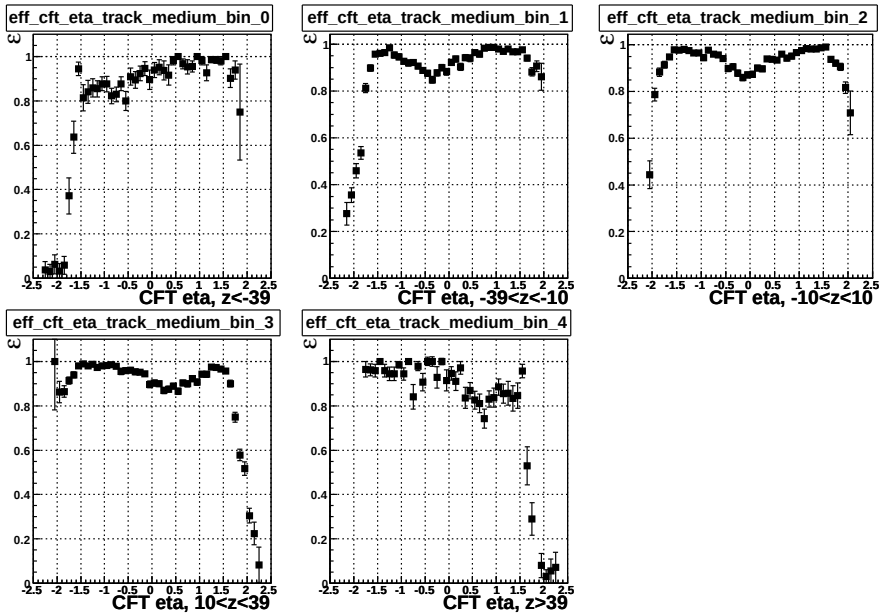

Figure 19: Tracking efficiency as a function of the reconstructed z position at dca of the muon. Only medium or better tracks are considered.

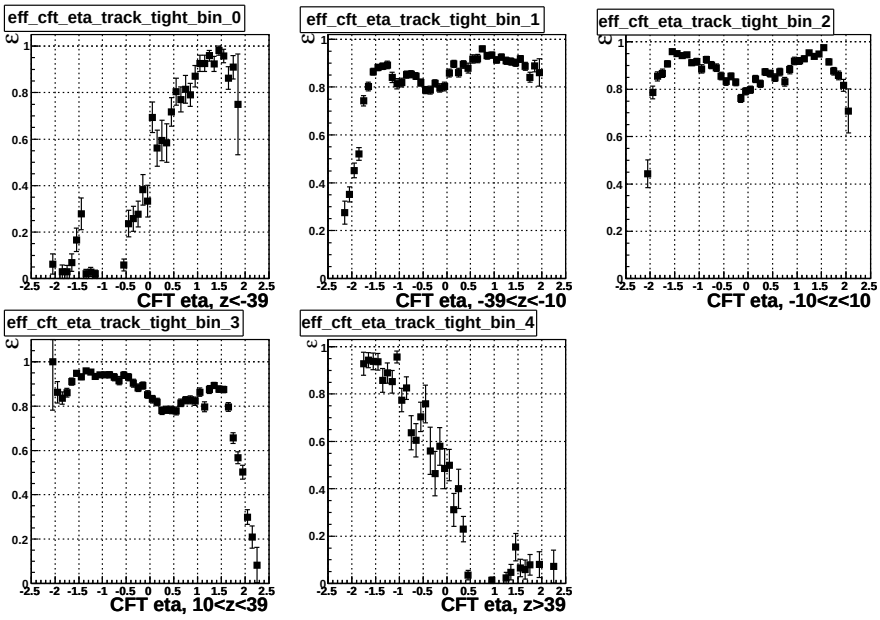

Figure 20: Tracking efficiency as a function of the reconstructed z position at dca of the muon. Only tight tracks are considered.

6.3.2 Time dependence and luminosity dependence

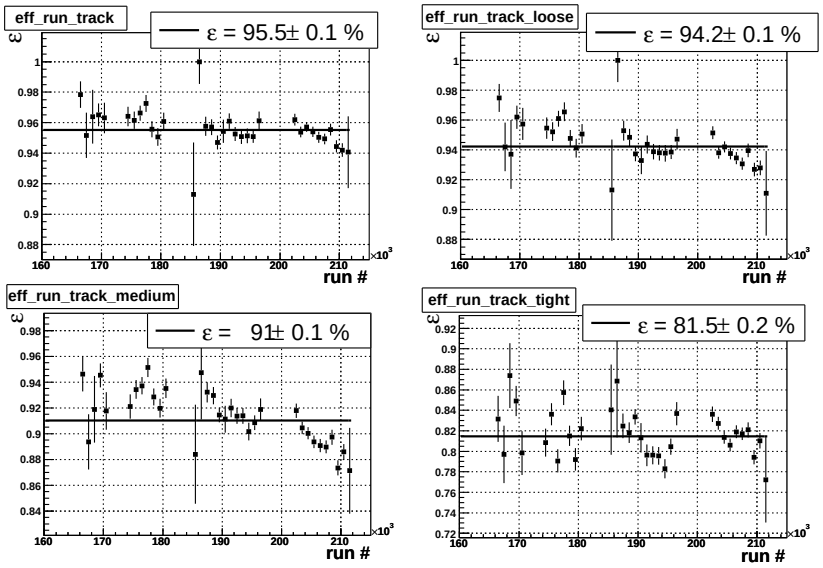

Figure 21: Evolution of tracking efficiency along time for various track quality.

Figure 21 shows the dependence of the various tracking criteria as a function of the run number. Variations of magnitude ±2% are observed. The magnitude of variation for the luminosity dependence, displayed in Figure 22 is $\simeq 10\%$ over the full luminosity range.

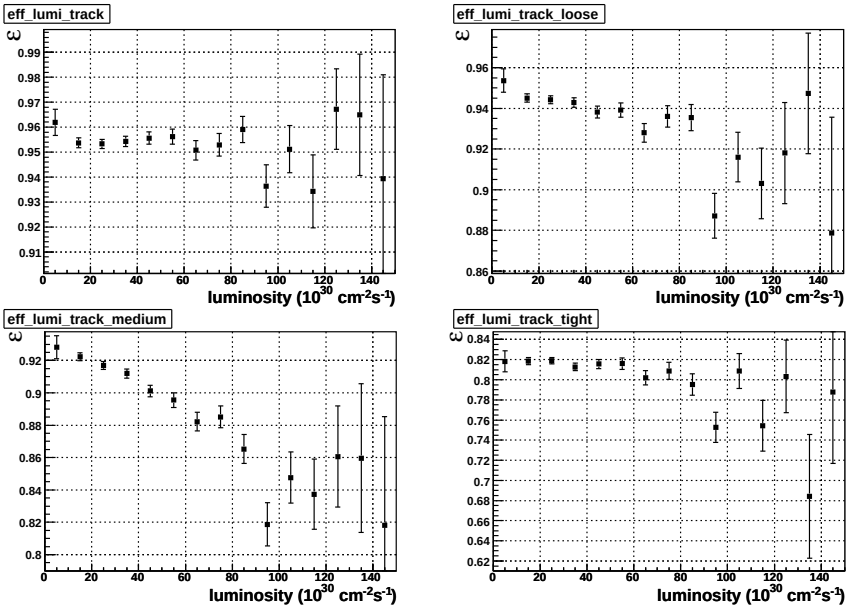

Figure 22: Tracking efficiency Vs instantaneous luminosity for various track quality.

In order to disentangle time and luminosity effect, Figure 23 shows the efficiencies for the criteria (loose), (medium relative to loose), (tight relative to medium) for pre and post-shutdown 2004 data. To remove the effect of beam narrowing the control track are required to have $|z| < 30$ cm.

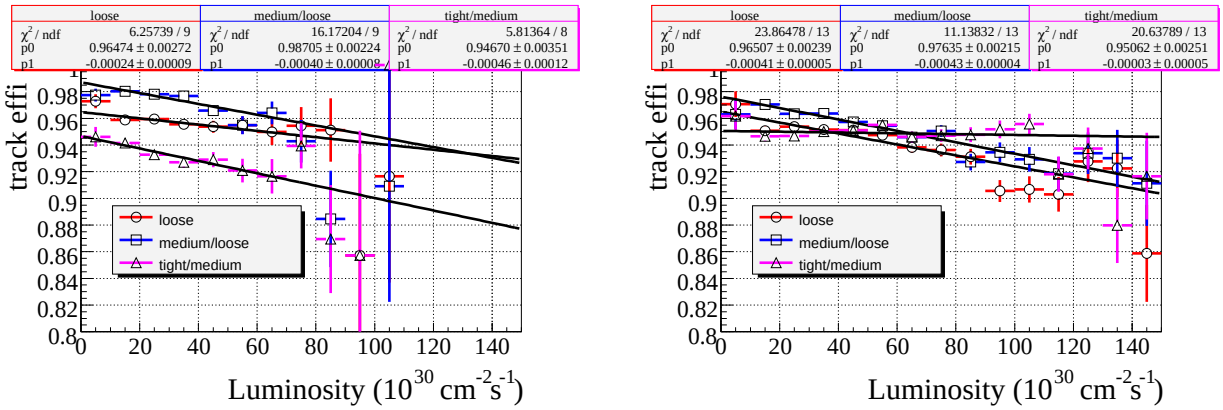

Figure 23: Dependence of the tracking efficiencies with respect to the instantaneous luminosity. On the left pre-shutdown 2004 data. On the right post-shutdown 2004 data. The efficiency has been computed for (loose), (medium relative to loose) and (tight relative to medium) for tracks with $|z| < 30$ cm..

It is observed that both the absolute values and the slopes of loose and (medium/loose) efficiencies are worse in the most recent data. The differences in absolute values and slopes may indicate some issues at the detector level after 2004 shutdown (eg: detector misalignment).

There is no satisfactory explanation at the moment. This may be related to the degradation of momentum resolution discussed in section 9.

When the study is repeated on the certification MC sample ($Z \rightarrow \mu^+\mu^-$ MC events with zero bias overlaid), no slope is observed as a function of the instantaneous luminosity of the overlaid events. This is shown in Figure 24. Thus, explaining the slope by saturation in CFT electronics or track picking spurious hits at high luminosity does not seem to be right.

It is worthwhile to notice that the degradation with luminosity is more pronounced at $\eta \simeq 0$ as can be seen in Figure 25.

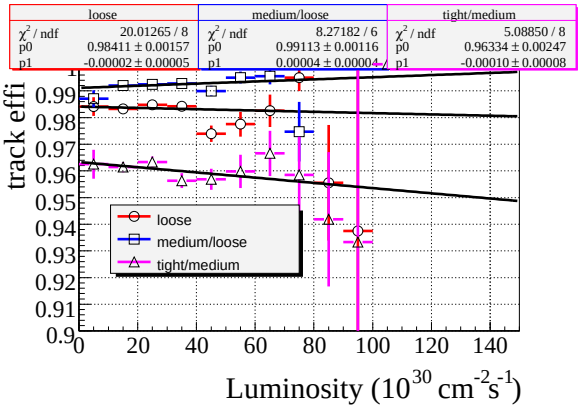

Figure 24: Dependence of the tracking efficiencies in MC with respect to the instantaneous luminosity of overlaid events.

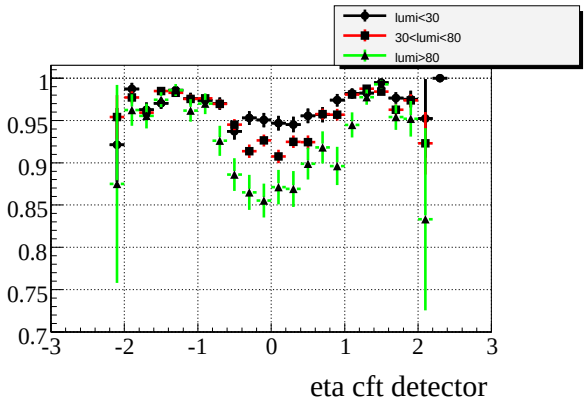

Figure 25: Efficiency of medium tracking with respect to loose tracking, for post-shutdown 2004 data, for low, moderate and high instantaneous luminosity.

6.3.3 DATA/MC ratio

The tracking efficiencies are found to be different in data and MC. This can be seen in Figure 26 where the $\varepsilon(DATA)/\varepsilon(MC)$ ratios as a function of CFT detector η are shown.

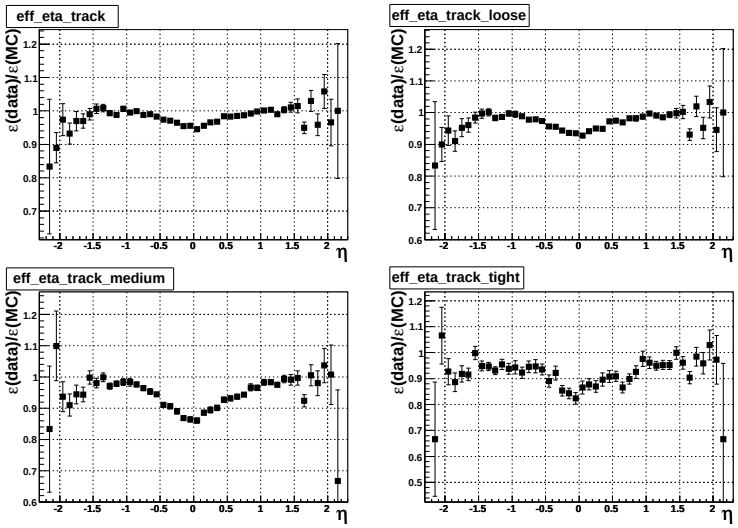

Figure 26: Ratio of data and MC tracking efficiencies as a function of pseudorapidity for various quality criteria.

For CAF analysis, the tracking efficiencies has been computed in 2-dimension, as a function of CFT detector η and z of the muons by the package muid_eff [7] for both data and MC. The binning is:
- in η 44 bins from -4.2 to 4.2.
- in z 5 bins (units in cm): $[-100, -39]$, $[-39, -10]$, $[-10, -10]$, $[10, -39]$, $[39, 100]$.

Typically, the average correction factors are respectively 0.96, 0.93 and 0.91 for respectively the loose, medium, and tight criteria.

6.4 Systematic uncertainty on the tracking efficiency corrections

Several sources of uncertainty may affect efficiency measurements and data/MC correction factors. We try to here to assess them quantitatively. For some specific reason, the reader may find that these numbers can not be applied straightforwardly to his analysis. So this part can also be viewed as a guideline.

6.4.1 tag and probe bias using MC

Existence of a possible bias in the method has been assessed here [13] (p14-pass1) by looking at the difference between the tag and probe measurements and the genuine efficiency in MC events. The bias is found to be 0.2% for a track quality criteria very close to track tight as defined in section 3.2. The study has not been repeated within p17 but the results are thought to remain valid.

As for muonid (Section 5.6.2) the bias would be expected to be the same for data and MC and should cancel in the ratio if there were no trigger condition in the event selection. As there is a trigger requirement in the data selection, we consider that a bias still exist and quote a 0.2% systematic uncertainty for the ratio DATA/MC.

6.4.2 background contamination

Presence of background in the data may bias downward the efficiency. Possible background may be for example QCD (tag=muon in jets, probe=jet faking muon) or $W \rightarrow \mu\nu$ (tag=high p_T muon, probe=fake muon).

To assess background effect we vary some cuts, that are supposed to change the contamination in background events. The resulting variation may also be due to the tag and probe biases. Thus we also determine the effect of the cut variation in MC events to correct for it.

1. Constraining the tag and probe to be back to back ($\Delta\varphi > 2.9$) yields a relative variation of 0.3%, 0.3% and 0.4% for respectively the loose, medium and tight tracking efficiency.

   A smaller variation is observed in the MC: 0.2%, 0.3% and 0.2% for respectively the loose, medium and tight tracking efficiency.

   The difference between data and MC is kept as a systematic which yields: 0.1%, 0% and 0.2% for respectively the loose, medium and tight tracking efficiency.

2. Constraining the events to have no reconstructed jet, an increase of of 0.2%, 0.4% and 0.4% for respectively the loose, medium and tight tracking efficiency.

   In the MC the correspondig variation are respectively 0%, 0% and -0.1%. The difference between data and MC is kept as a systematic which yields: 0.4% for the loose, medium and tight tracking efficiency.

   Note that if we are contaminated by QCD events, this cut is supposed to reduce them.

3. Tightening the dca cut of the control muon to 0.1 cm, no sizeable variation is observed.

This series of results demonstrate that the contamination in background is small. However it is not certain that the observed variations are really due to presence of background. Nevertheless

the variations are summed quadraticaly which yields an uncertainty of 0.4% for tight, medium and loose tracking.

6.4.3 Time and luminosity

Bias in measurement: As observed in section 5.3 and 5.4, the variations as a function of time and luminosities are as large as a few percents and they yield a correlation between the tag and the probe muon. This correlation may bias the efficiency measurement because the tag and probe selection involves tracking requirements which modify the luminosity profile of the sample.

To assess this bias, the efficiency as a function of luminosity is convoluted with different luminosity profiles arising from different $Z \rightarrow \mu^+\mu^-$ selections: we use the tag and probe selection for tracking efficiency measurement, the tag and probe selection for muonid efficiency measurement and the tag and probe selection for isolation efficiency measurements. We observed relative variation of the convoluted efficiency for the loose, medium and tight criteria. The largest variations are $\simeq 0.2\%$. This number is quoted as a systematic error. Note that the same procedure has been repeated using the run number distribution instead of the luminosity profile. Same variations, 0.2% at most are obtained.

Using average efficiency instead of time dependent efficiency: The efficiencies provided in the muid_eff package are averaged over the full data set according the wzreco selection. This average may be not suitable for all analysis.

For example, one can imagine an analysis for which the trigger efficiency in v14 trigger list is higher than in v13 triggerlist. Then the right average over time of tracking efficiency would require to put more weight on data corresponding to the v14 triggerlist than in wzreco data.

To assess the bias arising from this kind of problem, we use a typical (and somewhat extreme) example: we weight 20% more the post-shutdown 2004 period (v13 v14 triggerlist) than what comes out of wzreco. This example would correspond to a 20% variation of trigger efficiencies between v12 and v13-14. To remove beam width dependency we also employ the cuts $|z_{tag}| < 30$ cm. With respect to the standard average the obtained efficiencies are lower by 0.1%, 0.1%, 0.1%, respectively for the loose, medium and tight tracking criteria.

6.4.4 Choice of binning

The efficiency corrections are parameterized in a binned 2d map, as described Section 6.3.3

By doubling or halfing the size of the binning in both the η and z directions, or using a uniform 5 cm-width binning in z, and convoluting with the proper η z track distribution, no more than 0.15% variation is observed for the loose medium and tight tracking efficiency ratio.

6.4.5 φ isotropy

Since well reconstructed muons are used as probe, and because of the bottom muon hole, we cannot obtain a uniform φ coverage for the tracking efficiency measurement. By computing the efficiency in (z,η) map we average out the possible φ variations. Such variations are expected to happen for example because of different length of the optical fiber as a function of φ for the

CFT detector. The dead channel pattern of the SMT detector is also far from being uniform in φ as seen in Figure 10.

To assess the uncertainty due to the average over φ, the 2d efficiency maps as a function of (η, φ) are computed using the cut $|z| < 30$ cm to get rid of the z dependence of the efficiencies. The (η, φ) tracking correction maps are then convoluted with the (η, φ) distributions of reconstructed $Z \rightarrow \mu^+\mu^-$ MC muon. Comparing results with 30 bins and with 1 bin along φ yield differences of 0.2% for the loose medium and tight tracking criteria. This 0.2% is taken as a systematic uncertainty.

6.4.6 z vertex simulation

The tracking efficiency is highly dependent upon the z of the primary vertex. The MC has been simulated using a fixed gaussian distribution of width 25 cm. Studies demonstrate that this is a crude approximation [14]. The width of the luminous region along z depends both upon the run period and the instantaneous luminosity. Because the MC is generated with the wrong distribution it needs to be properly reweighted otherwise the tracking acceptances are wrong. On average the real shape is wider than the default MC shape. Thus more events are outside the z acceptance of the tracking system.

To assess the effect of wrong primary vertex simulation, we first compute the average shape of the beam by convoluting the function $beam(z, lumi, run)$ from [14] with the $(lumi, run)$ distribution of the wzreco data sample. The results of this convolution is shown in Figure 27 where it is compared to default MC shape.

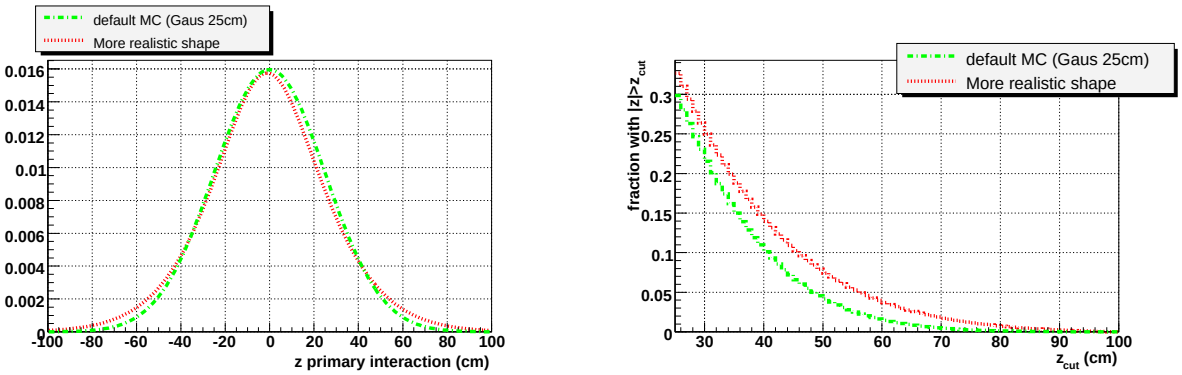

Figure 27: On the left comparison of the average beam shape with the default MC beam shape. On the right, these functions are integrated to determine the fraction of events having $|z| > z_{cut}$.

The shape of the beam is used to reweight the $(\eta, z)_{MC}$ distribution of $Z \rightarrow \mu^+\mu^-$ MC muons passing respectively the loose medium and tight tracking criteria. The resulting distribution is convoluted with the (η, z) efficiency correction factor to obtain the MC acceptance.

This results is compared to what is obtainend when no beam correction is applied. Without beam width correction the tracking acceptance is seen to be overestimated by 2.1%, 2.2% and 3.9% relative for respectively the loose, medium and tight tracking criteria.

We quote these large numbers as systematic uncertainties since at the time being most of the analysis do not correct for the beam shape simulation.

6.4.7 limited statistics

The limited size of both MC and data samples yields a stastical uncertainty for the data/MC correction. It amounts to 0.1%, 0.2% and 0.2% for respectively the loose medium and tight tracking criteria.

6.4.8 Summary

In Table 4, the figures about systematic uncertainty regarding the tracking correction factors are summarized. As the CAF correction utilities already accounts for the statistical uncertainties, it is not added to the total.

The results with or without beam shape systematic uncertainty (which is actually a real shift) are quoted.

Source of systematic	loose	medium	tight
tag and probe bias	0.2%	0.2%	0.2%
background and cut variations	0.3%	0.6%	0.6%
luminosity and time bias	0.2%	0.2%	0.2%
time average	0.1%	0.1%	0.1 %
finite binning	0.15 %	0.15 %	0.15 %
average over φ	0.2 %	0.2 %	0.2 %
simulation of beam along z	2%	2%	4%
data and MC stat	0.1%	0.2%	0.2%
Total w/o stat	2.2%	2.3 %	4 %
Total w/o stat and beam	0.5 %	0.7 %	0.7 %

Table 4: Summary of systematic uncertainties on tracking correction factors

6.5 Efficiency correction and systematic summary for tracking

In Table 5, the typical average numbers are given. They may depend upon the topology and η φ distribution of the muons, so these are only indicative results:

Muon type	loose	medium	tight
Efficiency in data	94.2%	91%	81.5
DATA/MC correction	0.96 ± 0.022	0.93 ± 0.023	0.91 ± 0.04
DATA/MC correction w/o beam syst.	0.96 ± 0.005	0.93 ± 0.007	0.91 ± 0.007

Table 5: Figures for tracking efficiencies, correction factor and systematics

6.6 Isolation efficiency

6.7 Isolation Dependence on Luminosity

It has been found that the most common isolation definitions (calorimeter halo and track halo) have a dependence on instantaneous luminosity. Figure 28 come from the W $\rightarrow \mu\nu$ cross section analysis, and show the fraction of events passing the track and calorimeter isolation after applying all other cuts against the instantaneous luminosity (note, this is the average per bunch, so must be multiplied by 36 to get the overall average).

For the track isolation, the calculation implemented in p14/p16 MuoCandidate did not require a match in z between the muon track and the other tracks entering the calculation. The luminosity dependence can be removed by recalculating the track isolation requiring a 2 cm match in z (this is done by default in p17).

For the calorimeter isolation, the luminosity dependence is the result of pile-up in the calorimeter, and cannot be fixed so easily. Instead, a luminosity dependent cut produces a flat efficiency, for example, requiring calorimeter halo $< 2.4 + 0.57 \times \mathcal{L}$ GeV rather than < 2.5 GeV. A better alternative may be to implement a dependence on the number of interactions (number of reconstructed vertexes) in the event, but so far this has not been studied. Figure 28 also shows the luminosity dependence using the updated definitions.

Figure 28: Histogram showing, as a function of instantaneous luminosity, the fraction of events passing the calorimeter and track isolation cuts after all other cuts have been applied, from the W $\rightarrow \mu\nu$ cross section analysis. Figures (a) and (b) show the 'standard' calorimeter and track isolation definitions, (c) and (d) show the updated definitions (described in the text).

6.8 Isolation Cuts Efficiency And Scale Factors

This section shows the efficiency for $Z \rightarrow \mu\mu$ data and MC for each isolation working point. The efficiency was measured on $Z \rightarrow \mu\mu$ data using a tag and probe method similar to what is described in section 6.1.2. For the probe muon to be considered in the efficiency measurement, the tag muon is require to pass the following isolation requirement to remove any heavy flavor background as a possible bias.

- TrackHalo < 3.5 GeV and CalorimeterHalo < 2.5 GeV.

The tag and probe muons used for the efficiency measurement were also required to have a mass consistent with a Z decay ($70 < M_{\mu\mu} < 110$ GeV).

The following sections show the isolation cut efficiency on a $Z \rightarrow \mu\mu$ data sample as function of several variables. Next to the efficiency plot is the data to Monte Carlo scale factor.

Similar isolation cuts are grouped together to limit the number of plots. For the following plots, there are three groups.

- "TopLoose": TopScaledUltraLoose, TopScaledVeryLoose, TopScaledLoose, and TopScaledMedium
- "TopTight": TopScaledTight, TopScaledVeryTight, TopP14, and DeltaR(μ,jet)

- "NP": NPLoose and NPTight

6.8.1 Muon P_T Dependence

6.8.2 Muon η Dependence

6.8.3 Number of Jets Dependence

6.8.4 ΔR(μ,jet) Dependence

6.8.5 Time Dependence

6.8.6 Vertex Multiplicity Dependence

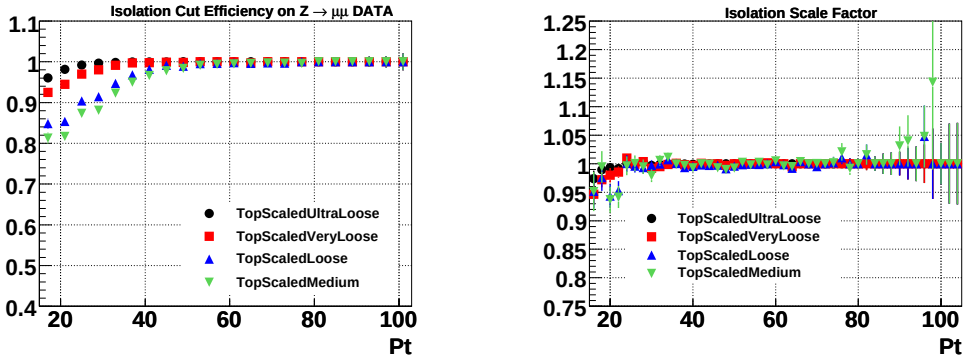

(a)

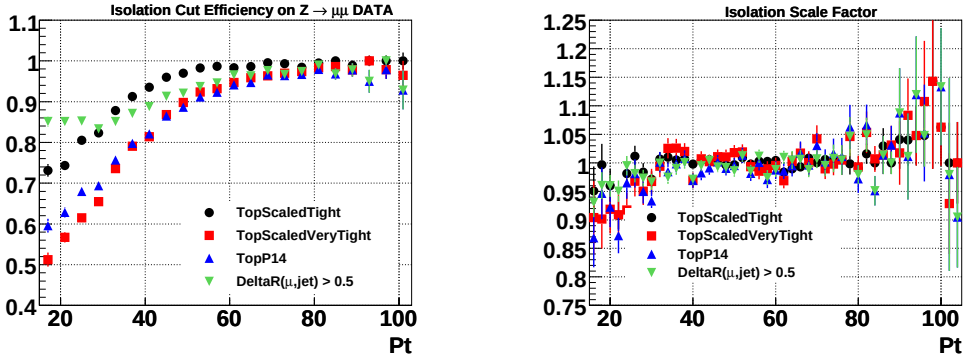

(b)

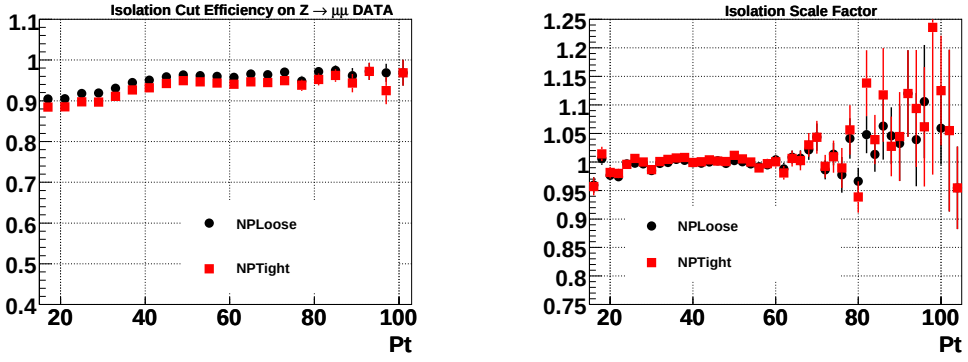

(c)

Figure 29: Isolation cut efficiency versus muon p_T on a $Z \rightarrow \mu\mu$ data sample (left plots) and data/MC scale factors (right plots) for "toploose" group (a), "toptight" group (b), and "np" group (c).

6.9 Systematic Errors

6.9.1 Luminosity Dependence

Because the different isolation working points' efficiencies behave differently as luminosity increases it is important consider this dependence as a possible systematic error in an analysis.

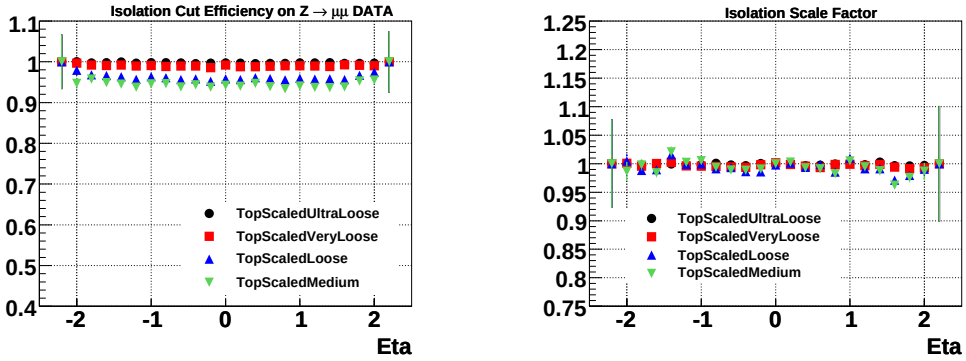

(a)

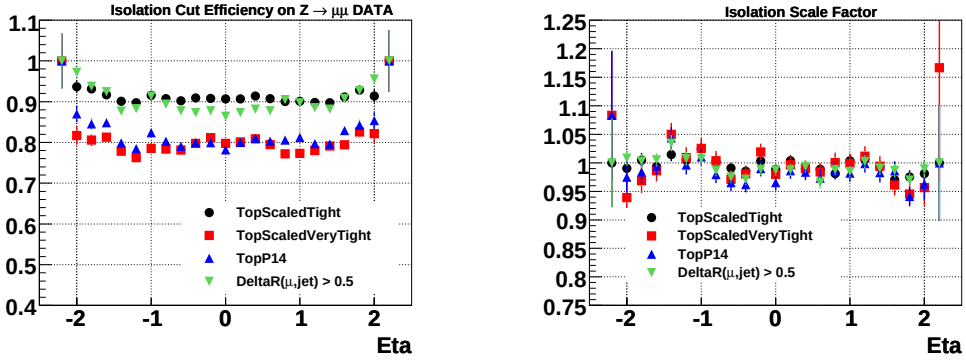

(b)

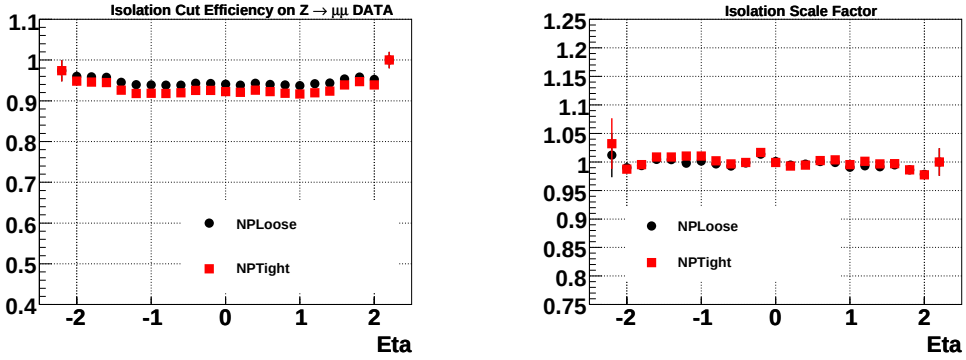

(c)

Figure 30: Isolation cut efficiency versus muon physics η on a $Z \rightarrow \mu\mu$ data sample (left plots) and data/MC scale factors (right plots) for "toploose" group (a), "toptight" group (b), and "np" group (c).

The "toploose" isolation cuts all show a negligable dependence on the number of reconstructed vertices. The topscaledloose efficiency is relatively constant until there are 8 vertices

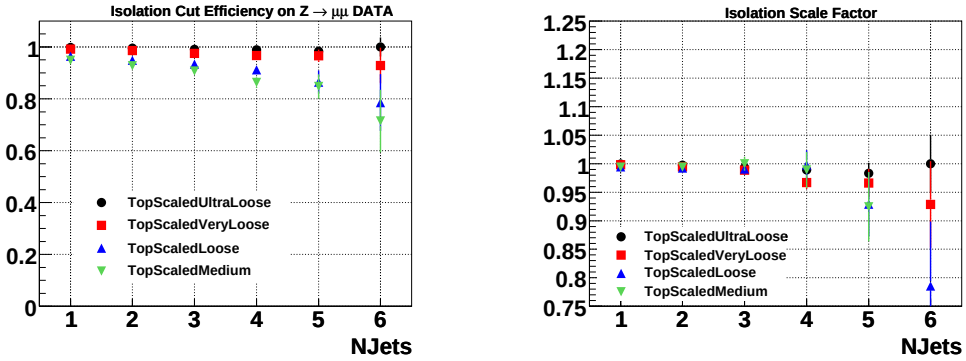

(a)

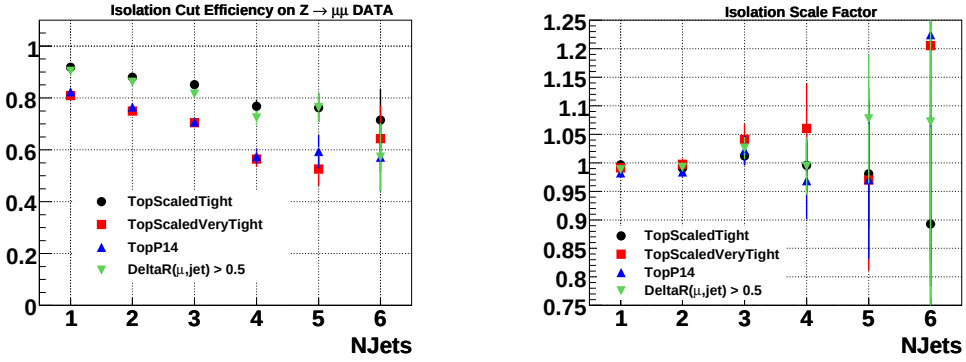

(b)

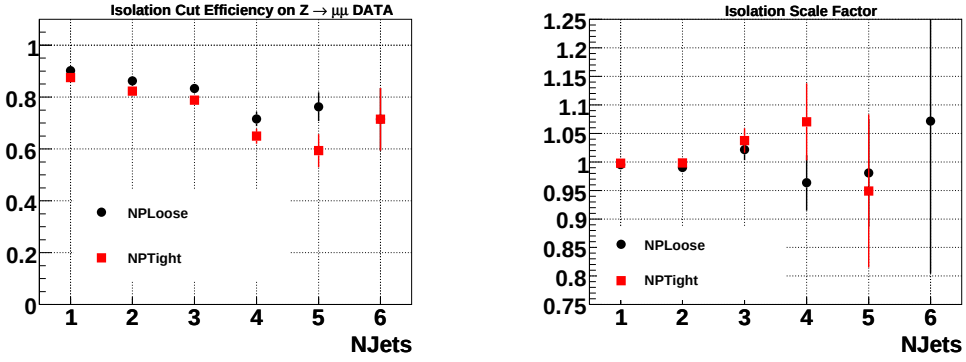

(c)

Figure 31: Isolation cut efficiency versus number of jets with $E_T > 15$ GeV on a $Z \to \mu\mu$ data sample (left plots) and data/MC scale factors (right plots) for "toploose" group (a), "toptight" group (b), and "np" group (c).

in the event. Also, the efficiency as a function of vertex multiplicity for the $Z \to \mu\mu$ MC seems to agree quite well with data.

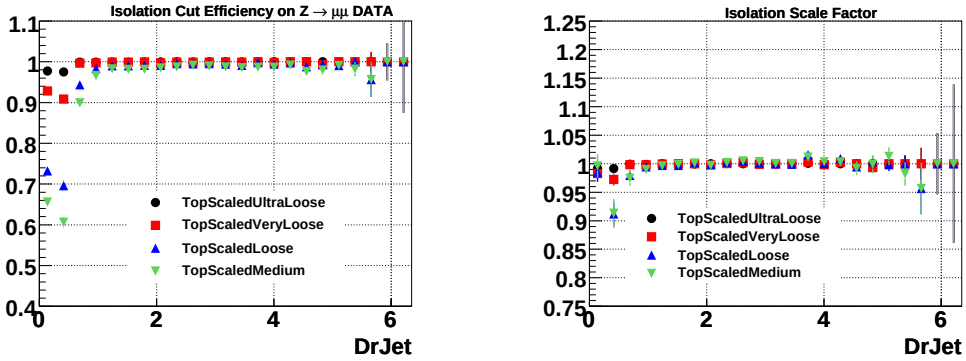

(a)

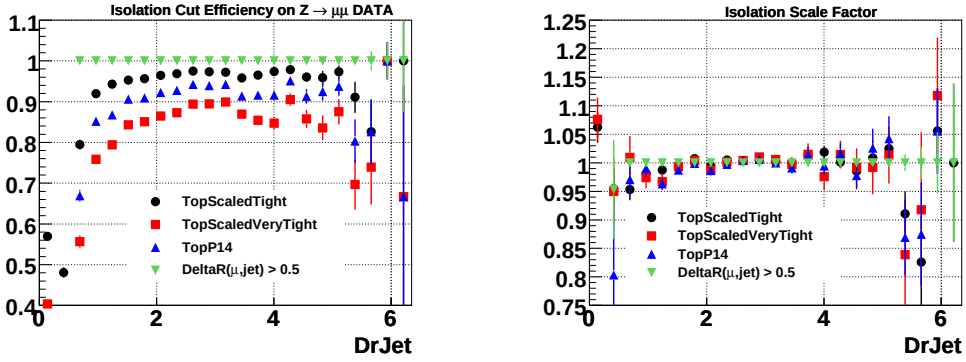

(b)

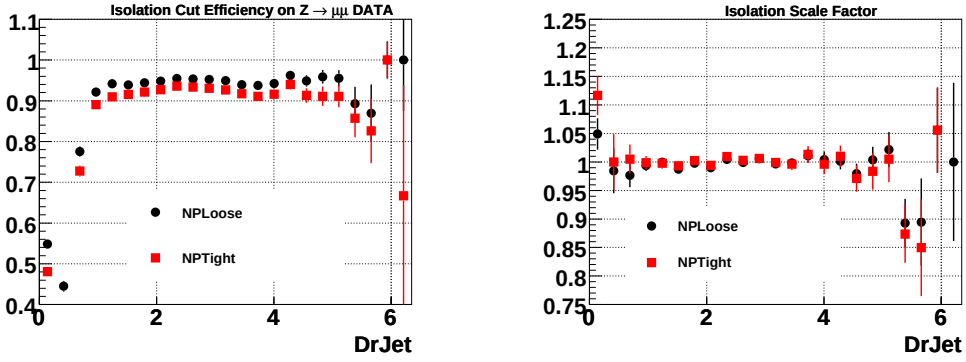

(c)

Figure 32: Isolation cut efficiency versus ΔRμ,closest jet, on a $Z \rightarrow \mu\mu$ data sample (left plots) and data/MC scale factors (right plots) for "toploose" group (a), "toptight" group (b), and "np" group (c).

The "toptight" isolation cuts show a stronger dependence on luminosity because these cuts require less calorimeter cell energy surrounding the muon and the cell energy baseline increases

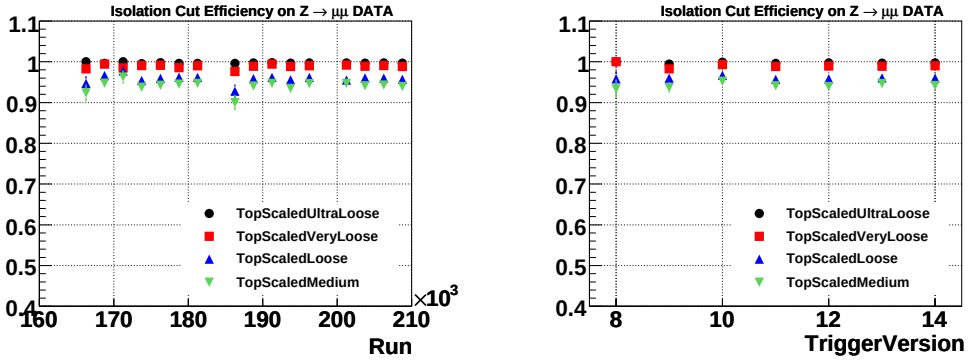

(a)

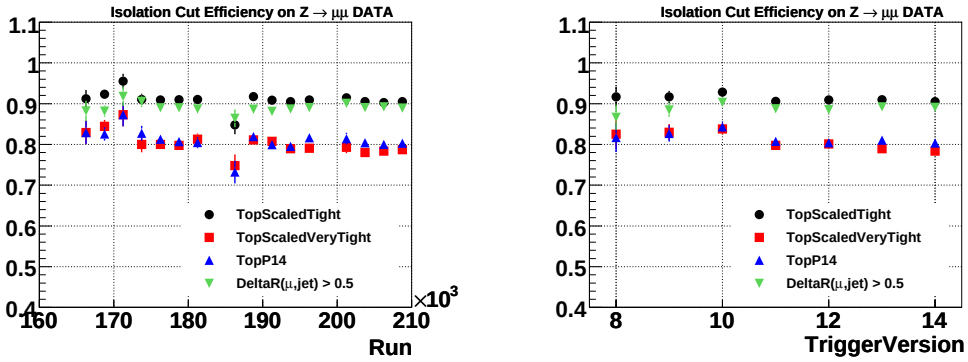

(b)

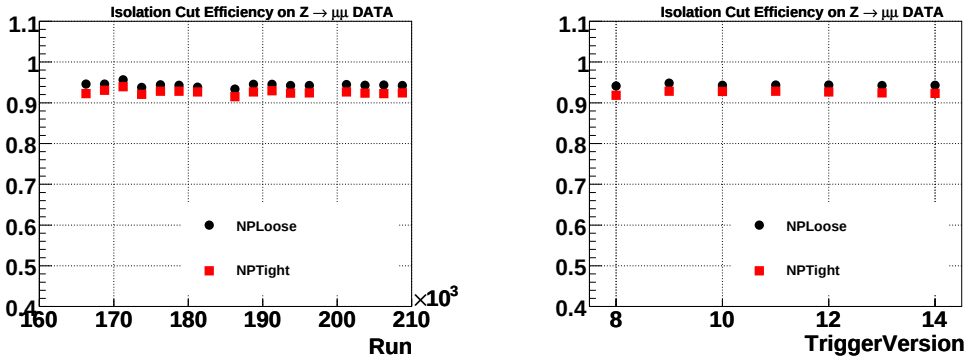

(c)

Figure 33: Isolation cut efficiency on a $Z \rightarrow \mu\mu$ data sample version run number (left plots) and trigger version (right plots) for "toploose" group (a), "toptight" group (b), and "np" group (c).

as luminosity increases. The topp14 isolation cut has the strongest dependence in this group although the efficiency is well modeled MC until there are 6 vertices in the event. For 6 vertices,

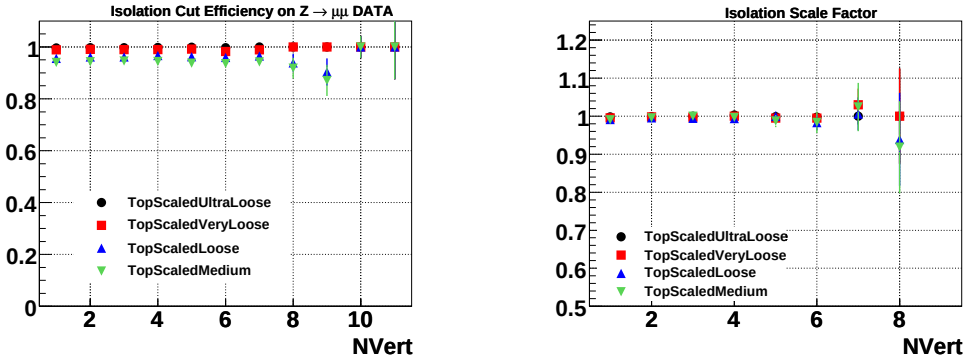

(a)

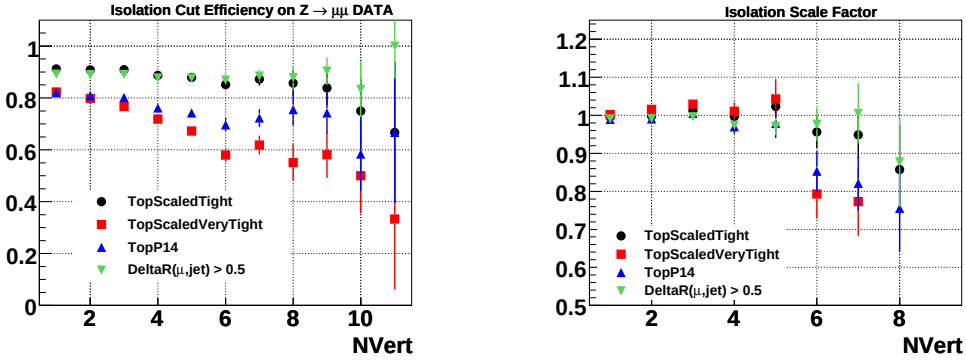

(b)

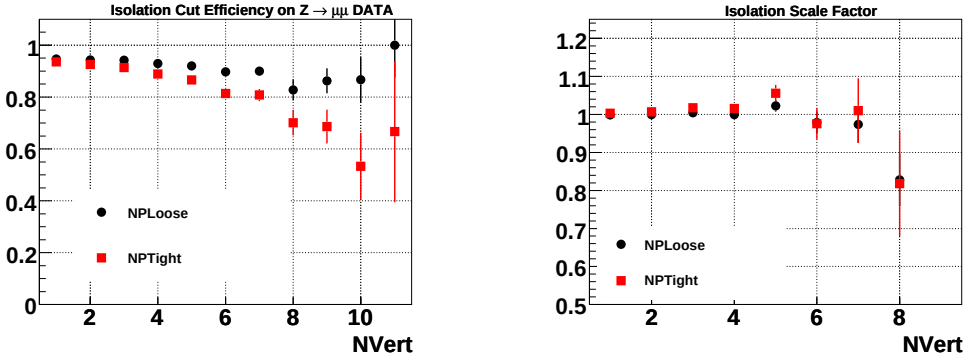

(c)

Figure 34: Isolation cut efficiency on a $Z \rightarrow \mu\mu$ data sample (left plots) and data/MC scale factors (right plots) for "toploose" group (a), "toptight" group (b), and "np" group (c).

the topp14 working point scale data/MC scale factor decreases to nearly 0.8, while other scale factors for this group decrease to roughly 0.9.

The "np" isolation working points also show a strong dependence on luminosity; however,

the dependence seems to be well modelled in the Monte Carlo. Only after 8 vertices, does the NPTight working point scale factor begin decrease.

6.9.2 Trigger Version / Run Number

All isolation cuts have a negligable dependence on trigger version and run number as seen in figure 33.

6.9.3 Z Boson Production vs Top Quark Production

Another potential source of systematic error is to take efficiencies derived in a $Z + 0$jets environment and apply those efficiencies to a multijet event, such as a top quark event. It can be seen in figure 31 that the isolation efficiency varies stronly a function of jet multiplicity. If the analyzer were to take efficiencies derived in the 0-jet bin, there would be an increasing overestimation of the efficiency as the number of jets increases. For example, from the plots in figure 31, it can be seen for the topp14 isolation working point, the efficiency in the 1-jet bin is 80% and the efficiency in the 4 jet bin is 59%. The data-to-Monte Carlo scale factor in this senario is 1.0 in the 1-jet bin and 1.08 in the 4-jet bin. Another common isolation working point is NPTight. If the jet multiplicity were ignored in the data-to-Monte Carlo ratio, the scale factor would artifially low by 10%.

7 trigger efficiencies for muons

The Level-1, Level-2 and Level-3 trigger efficiencies for muon related objects are computed using the tag and probe methods implemented in the packages wzreco/muo_cert [4]. The cuts used are exactly the same as for muid efficiencies, section 5.1, but the probe requirement is loosened from *track_medium* to *track_loose*.

For each term, the dependencies of the efficiencies are discussed. For some trigger terms it is neccessary to split the efficiencies into different trigger periods due to hardware or software changes. All plots shown here include the 'bottom hole' of the muon system, where the efficiency is considerably lower than for the rest of the muon system.

7.1 muon trigger

The muon triggers available in the p17 dataset come from the range of trigger lists v8 - v14.93.

7.1.1 Level-1 muon trigger

At level 1, there are two types of trigger terms, scintillator and wire based. At level 1, the trigger system is split into two regions, the 'wide' and 'all' regions. The all region is defined as $|\eta| < 2.0$. The definition of the wide region changed from $|\eta| < 1.5$ to $|\eta| < 1.6$ with the introduction of the v13 triggerlist. For this reason the efficiencies for the wide region trigger terms are split into two periods, before and after the introduction of v13.

The efficiencies for the Level one tight scintillator condition in the wide region as a function of detector eta and phi, relative to loose, matched offline muons, is shown in figure 35. The average efficiency in this sample for the tight scintillator is 78%. If one removes the hole the average inreases to 84%.

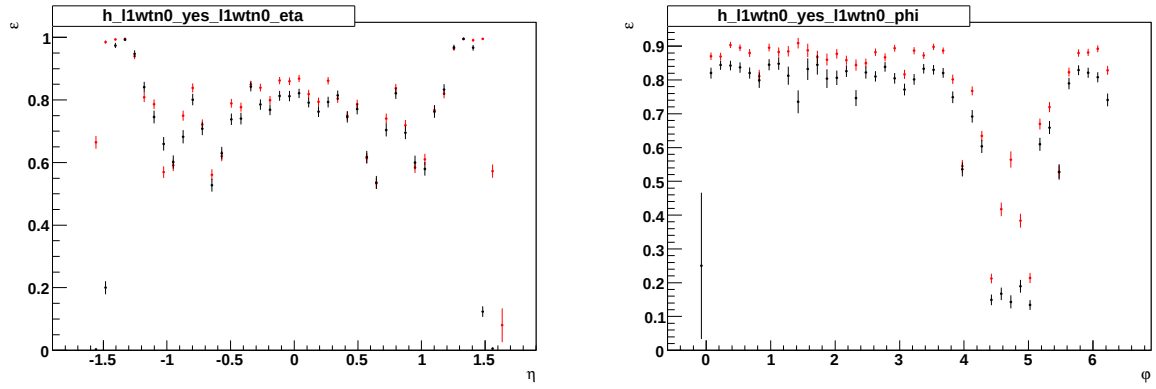

Figure 35: *The dependence of the Level 1 Tight Scintillator in the wide region on detector eta and phi, for data collected before triggerlist v13 (black) and data collectd with triggerlists v13 and v14 (red).*

The efficiencies for the level 1 loose wire condition in the wide region, as a function of detector eta and phi, relative to loose, matched offline muons that have fired the level 1 tight scintillator condtion, are shown in figure 36. Figure 37 shows the dependence on luminosity and

trigger version for data collected with the v13 and v14 triggerlists. The trigger term shows no dependence on luminosity. The sysytematic increase seen after trigger list version v13.20 can be explained by a bug fix for L1 muon, central octant 6 (see Trigger database). The average efficiency for the level 1 loose wire condition, relative to the level 1 tight scintillator condition in this sample is 95%. Of course it is necessay to paramaterize the level 1 efficiencies in terms of both eta and phi. Figure 38 shows the eta-phi efficiency maps for the level 1 tight scintillator and the level 1 loose wire, with respect to tight scintillator, in both cases in the wide region.

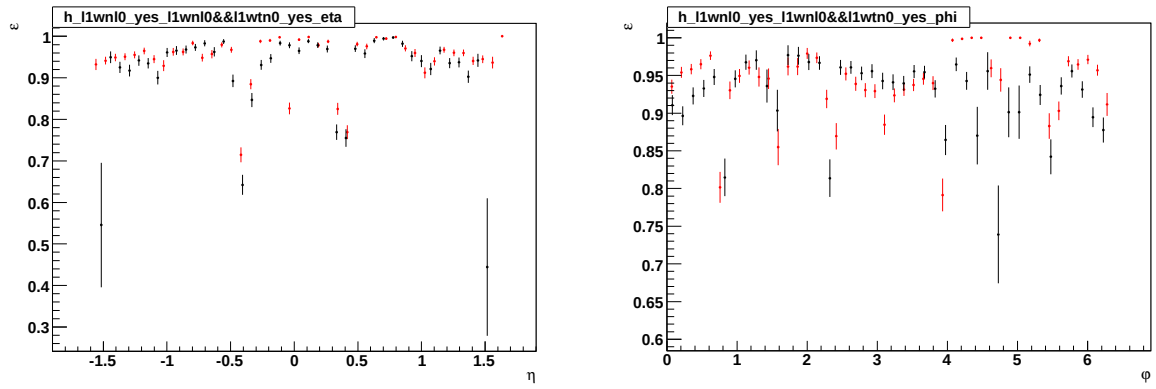

Figure 36: *The dependence of the Level 1 Loose Wire condition in the wide region, with respect to tight scintillator on detector eta and phi, for data collected before triggerlist v13 (black) and data collected with triggerlists v13 and v14 (red).*

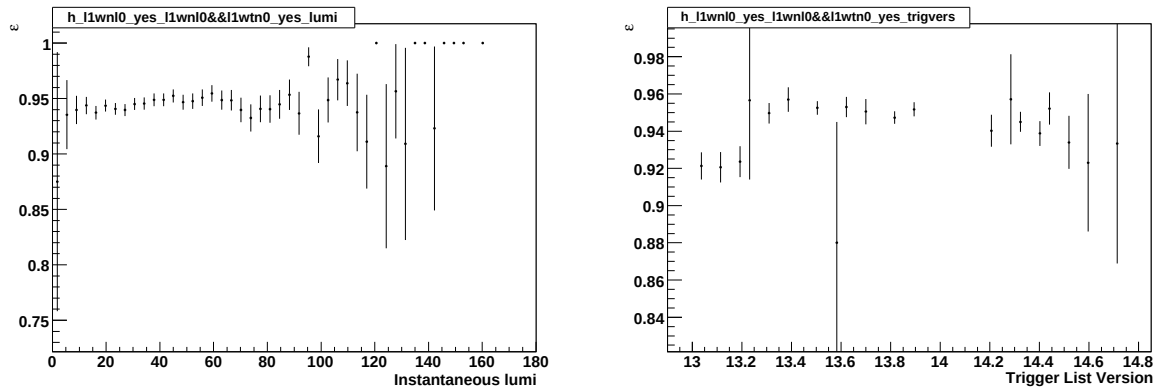

Figure 37: *The dependence of the Level 1 Loose Wire condition in the wide region, with respect to tight scintillator on instantansous luminosity and trigger version, for data collected with triggerlists v13 and v14.*

7.1.2 Level-2 muon trigger

At level 2, muons are classified as either loose, medium or tight. At level 2, the transverse momentum, obtained from the muon system can be required to be above a given threshold. Almost all the triggers use medium muons at level 2, with a p_T cut of 0, 3 or 5 GeV. Figure 39

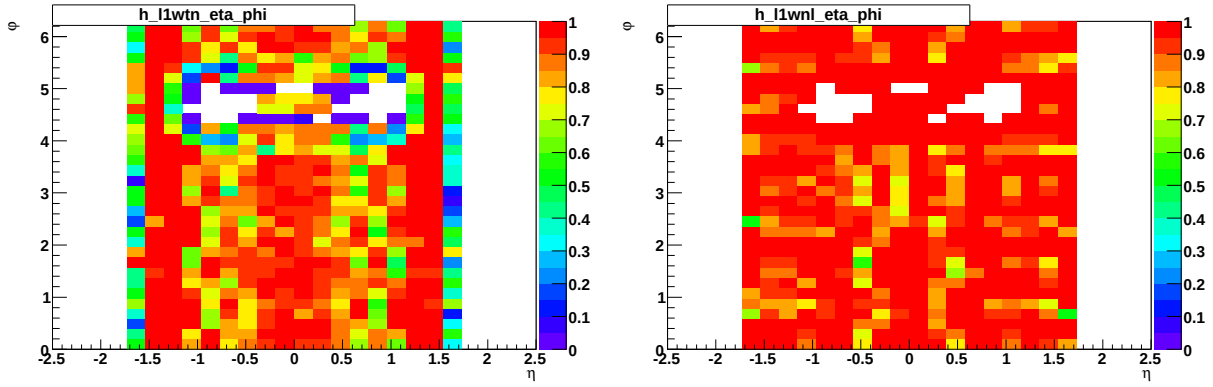

Figure 38: *The efficency maps showing eta and phi dependence for Level 1 Tight Scintillator (left) and level 1 loose wire with respect to the tight scintillator condition (right), for data collected with triggerlists v13 and v14.*

shows a typical eta, phi dependence, in this case for a level 2 medium muon, $p_T > 3$ GeV, with respect to loose offline muons that have fired the all region tight scintillator and loose wire level 1 trigger terms. The average efficiency for this term is 96%. The run and triggerlist dependence are shown in figure 40. This shows how for early data the trigger had lower efficiency.

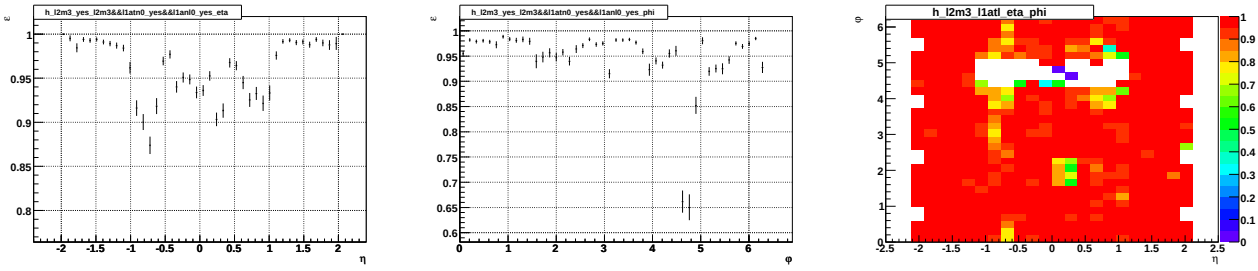

Figure 39: *The dependence of the Level 2, medium muon, $p_T > 3$ GeV requirement, with respect to loose offline muons that have fired the all region tight scintillator and loose wire level 1 trigger terms, on detector eta and phi.*

7.1.3 Level-3 muon trigger

The level 3 muon trigger was used for trigger lists v13 and v14. When run without track matching at level 3, the cut on the muon p_T is made using information from the local muon system. Figure 41 shows the dependence of level 3 loose muons, for $p_T > 15$ GeV and $p_T > 0$ GeV on detector eta and phi, with respect to loose, matched offline muons that have fired the level 1 tight scintillator trigger in the wide region. The sizeable drop due to the p_T cut at level 3 is clearly visible, note that this drop is independent of the muon p_T, at least above the 20 GeV cut used in muo_cert. The trigger is very stable with repsect to luminosity and triggerlist version, as shown in figure 42 for the $p_T > 15$ GeV condition. Given this, there is no need to split this term into efficiencies for v13 and v14 triggerlists.

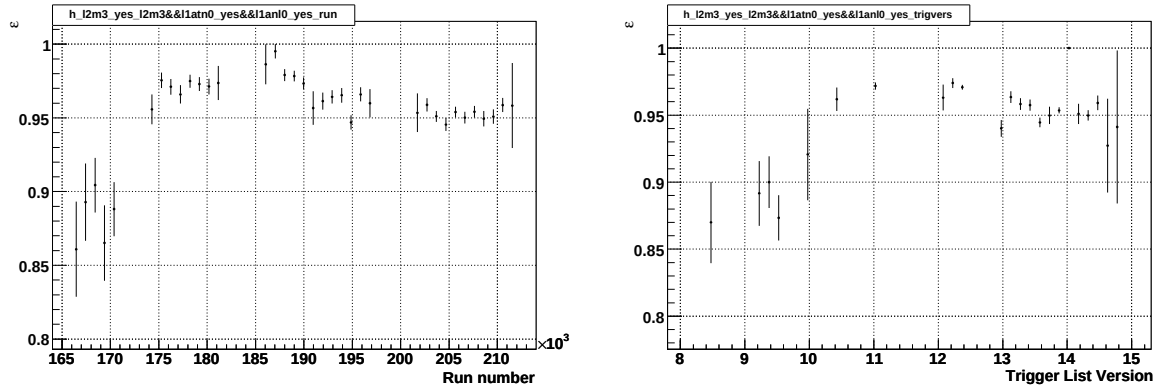

Figure 40: *The dependence of the Level 2, medium muon, $p_T > 3$ GeV requirement, with respect to loose offline muons that have fired the all region tight scintillator and loose wire level 1 trigger terms, on run and triggerlist version.*

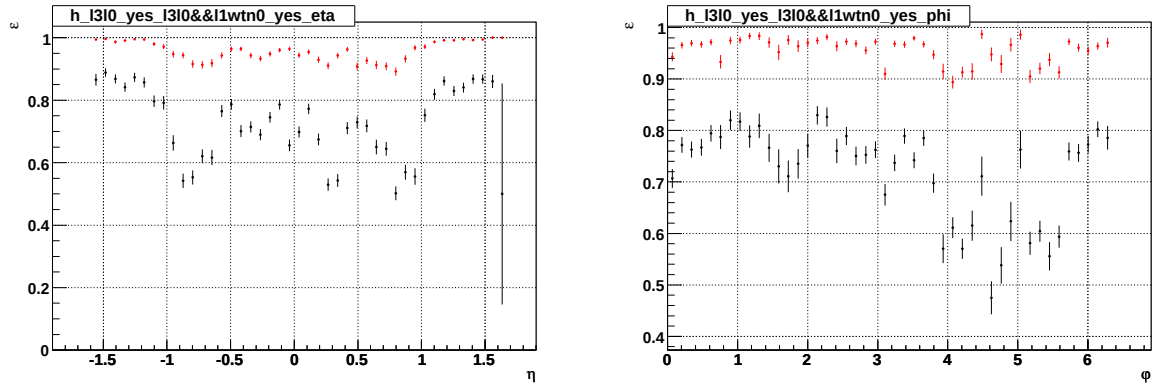

Figure 41: *The dependence of the Level 3 Loose Muon, $p_T > 15$ GeV (black) and $p_T > 0$ GeV (red), with respect to loose offline muons that fired the wide region tight scintillator condition, on detector eta and phi.*

Since the cut at Level 3 is made using the momentum of the local muon system, one expects a turn-on effect around the cut value. This has been studied for the case of Level 3 loose muon, $p_T > 15$ GeV. In order to study this effect, the p_T cuts in wzreco and muo_cert were lowered to 20 GeV for the tag muon and 15 GeV for the probe muon. The lower p_T cuts could bias the efficiency, since they may lead to increased background. The extent of the bias can be investigated a little. Figure 43 shows the efficiency of the Level 3 loose muon, $p_T > 15$ GeV, with respect to loose ofline muons that have fired the L1 tight scintillator condtion, for events where the tag has $p_T > 30$ GeV (black) and events where the tag has $p_T > 20$ GeV (red). The average efficiency changes from 0.7159 (for tags, $p_T > 30$ GeV) to 0.7130 (for tags, $p_T > 20$ GeV), a change of 0.4%.

The dependence of the Level 3 Loose Muon, $p_T > 15$ GeV term on offline p_T is shown in figure 44, along with 2 different fits of the turn-on curve. In the first fit an exponetial is used to modify the mean value (equation 2) and in the second a hyperbolic tangent is used (equation 3). The second fit is prefered, since the errors on the paramaters are smaller. To

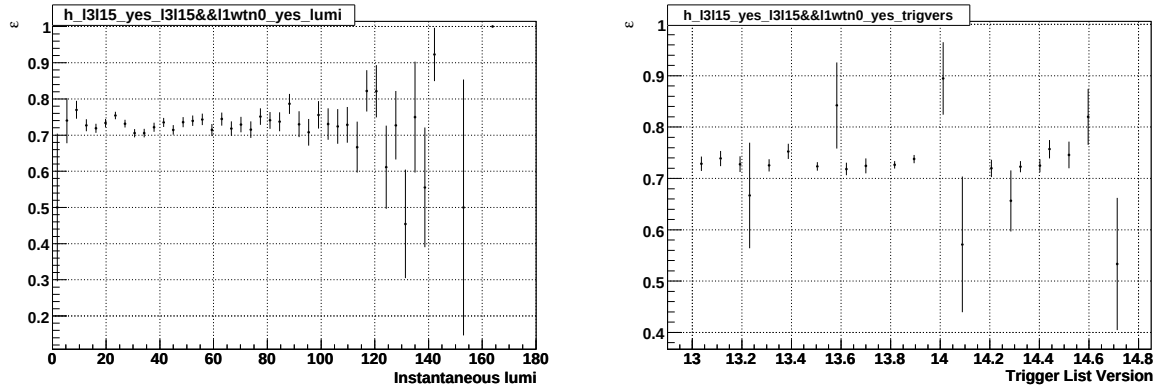

Figure 42: *The dependence of the Level 3 Loose Muon, $p_T > 15$ GeV, with respect to loose offline muons that fired the wide region tight scintillator condition, on instantaneous luminosity and triggerlist version.*

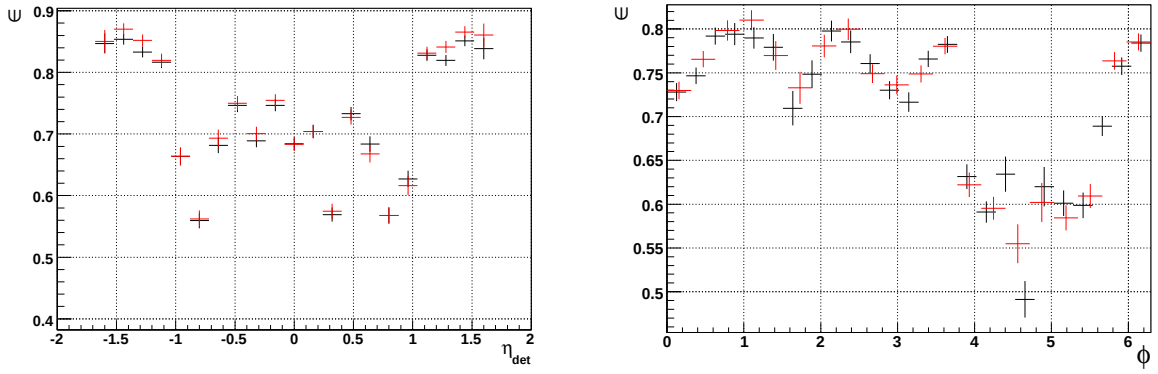

Figure 43: *The dependence on eta (left) and phi (right) for the Level 3 Loose Muon, $p_T > 15$ GeV condition, with respect to loose offline muons that fired the wide region tight scintillator condition. Red points are events where the tag muon has $p_T > 20$ GeV and black points are where the tag muon has $p_T > 30$ GeV.*

use either of the fit functions, one must assume the p_T dependence factorises from the eta-phi dependence. Under this assumption ϵ_0 can be taken from the standard eta-phi maps and then the fit function is used to correct the efficiency for the p_T of the muon. To test whether this approach works, figure 45 shows the p_T dependence for two different eta bins, $|\eta_{detector}| < 1.0$ and $|\eta_{detector}| > 1.0$. The fitted curve is overlayed, where parameters a and b are taken from the fit from the whole eta range and ϵ_0 is taken from the plateau of the curve. There are some deviations from the curve for the low eta case, which could be caused by the variable resolution of the local muon system.

$$\epsilon = \epsilon_0 * (1 - a * e^{-bp_T}) \tag{2}$$

$$\epsilon = \epsilon_0 * tanh(a * p_T - b) \tag{3}$$

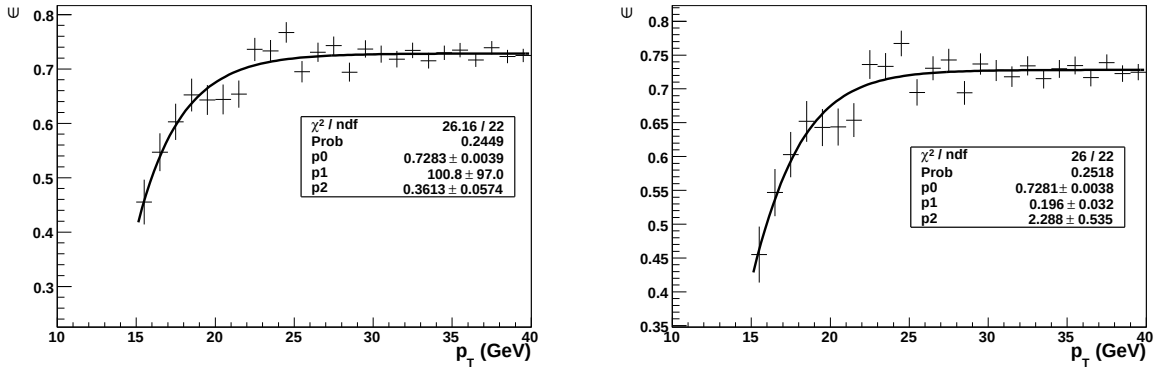

Figure 44: *The dependence on p_T for the Level 3 Loose Muon, $p_T > 15$ GeV condition, with respect to loose offline muons that fired the wide region tight scintillator condition. The curve is fitted with equation 2 on the left and equation 3 on the right.*

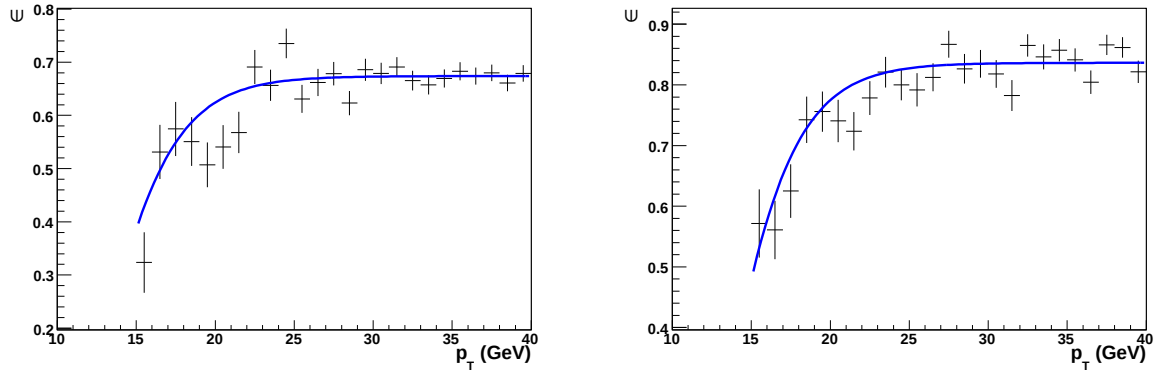

Figure 45: *The dependence on p_T for the Level 3 Loose Muon, $p_T > 15$ GeV condition, with respect to loose offline muons that fired the wide region tight scintillator condition. The left plot is for muons, $|\eta_{detector}| < 1.0$. The right plot is for muons, $|\eta_{detector}| > 1.0$.*

7.2 track trigger

7.2.1 Level-1 track

The level 1 track trigger was used in association with the level 1 muon triggers from triggerlist v13 onwards. Four different p_T bins are available for the L1 track trigger, the most important for single muon triggers is $p_T > 10$ GeV. The efficiency for level 1 tracks, $p_T > 10$ GeV as a function of phi, CFT detector eta and z is shown in figure 46. Is the phi dependence understood???

Figure 47 shows the efficiency for the same term as a function of instantaneous luminosity and triggerlist version. There is no dependence on luminosity, however there was a period of running (v13.2 - v13.4) where the term had systematically lower efficiency. This is not yet understood. The same effect is seen for level 1 tracks, $p_T > 5$ GeV, as shown by figure 48. Once the latest data is available it will be necessary to see if the introduction of singlet equations for the high p_T tracks has changed the efficiency significantly.

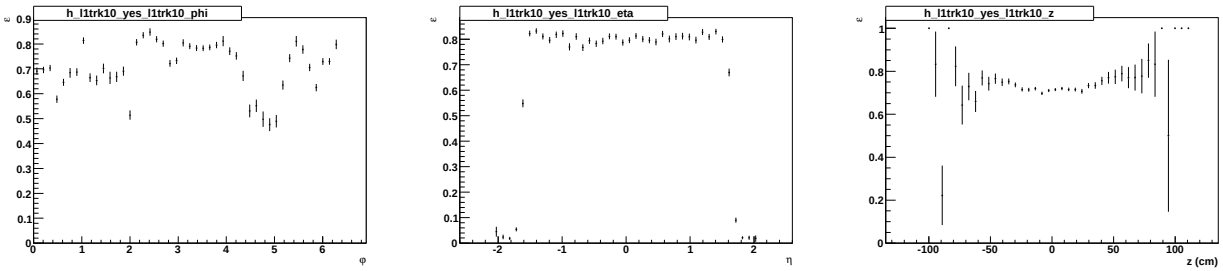

Figure 46: *The phi, CFT detector eta and z dependence of the Level 1 Track, $p_T > 10$ GeV term, relative to loose offline tracks.*

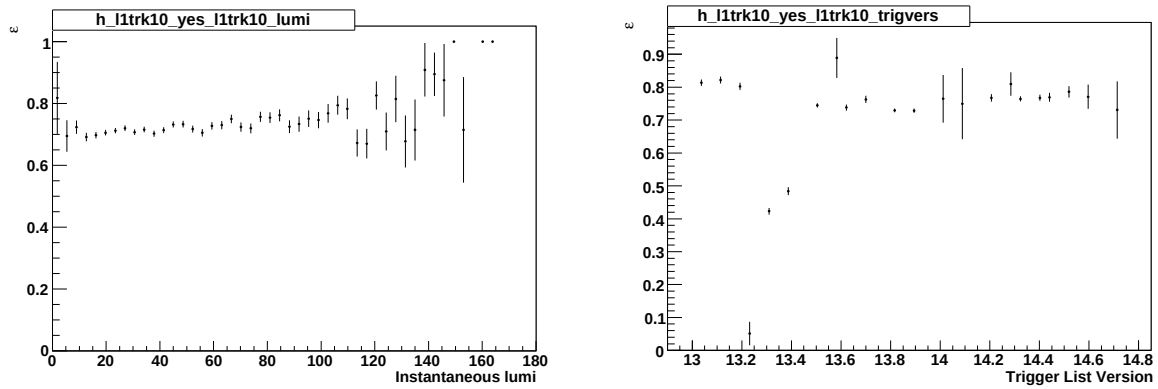

Figure 47: *The instantaneous luminosity and triggerlist version dependence of the Level 1 Track, $p_T > 10$ GeV term, relative to loose offline tracks.*

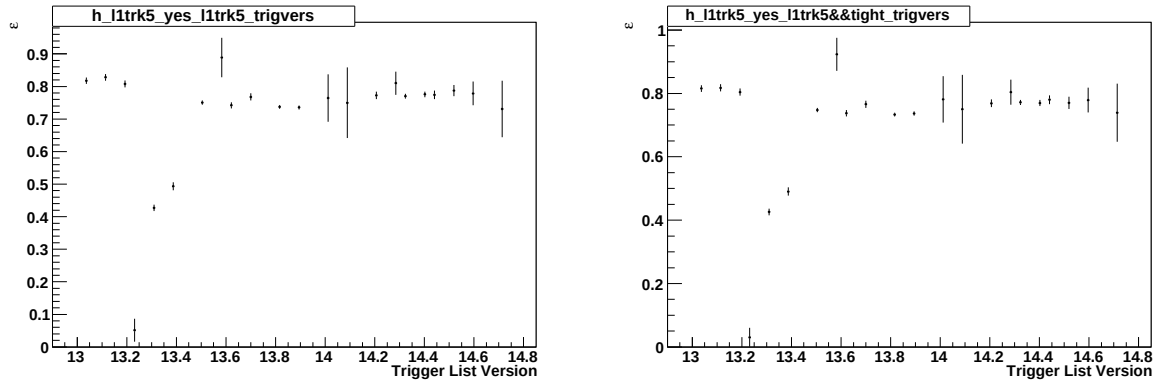

Figure 48: *The triggerlist version dependence of the Level 1 Track, $p_T > 5$ GeV term, relative to loose offline tracks (left) and tight offline tracks (right).*

7.2.2 Level-3 track

The level 3 track trigger was used for most of Run IIa. There was an important change that occured in the Level 3 tools at the start of the v14 triggerlist, after this point all level 3 tracks were required to have more than 10 hits, whereas previously the requirement had been for only

8 hits. Note that the 10 hit requirement implies 2 SMT hits, since only axial hits are used at level 3. The effect of this change can be seen in figure 49, which shows the dependence of the efficiency for level 3 tracks, $p_T > 10$ GeV, on triggerlist version. The figure shows a clear drop in efficiency co-inciding with the intriduction of v14. Note that the drop is smaller for the tight track offline definition, since here SMT hits are required offline.

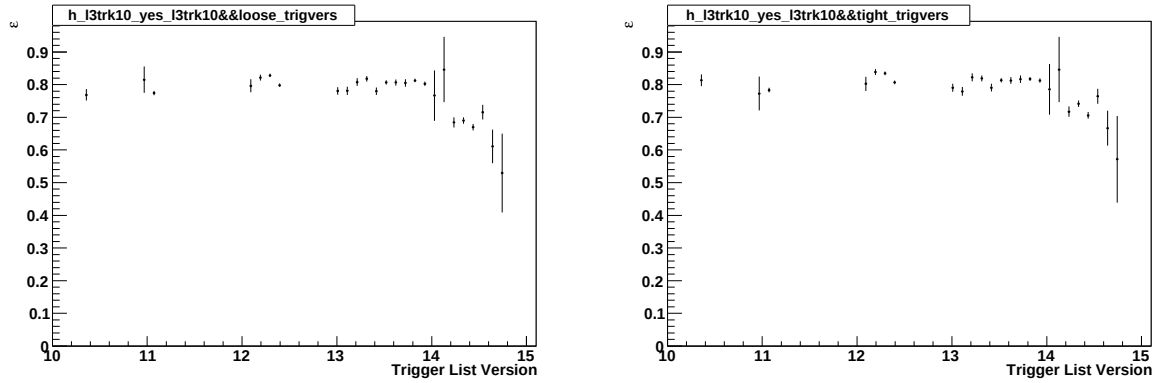

Figure 49: *The triggerlist version dependence of the Level 3 Track, $p_T > 10$ GeV term, relative to loose offline tracks (left) and tight offline tracks (right).*

The efficiency for level 3 tracks, $p_T > 12$ GeV, as a function of CFT detector eta and z, with respect to loose offline tracks that have fired the level 1 track, $p_T > 10$ GeV, term, is shown in figure 50. The difference between data collected before and after the introduction of the v14 trigger list is clearly visible.

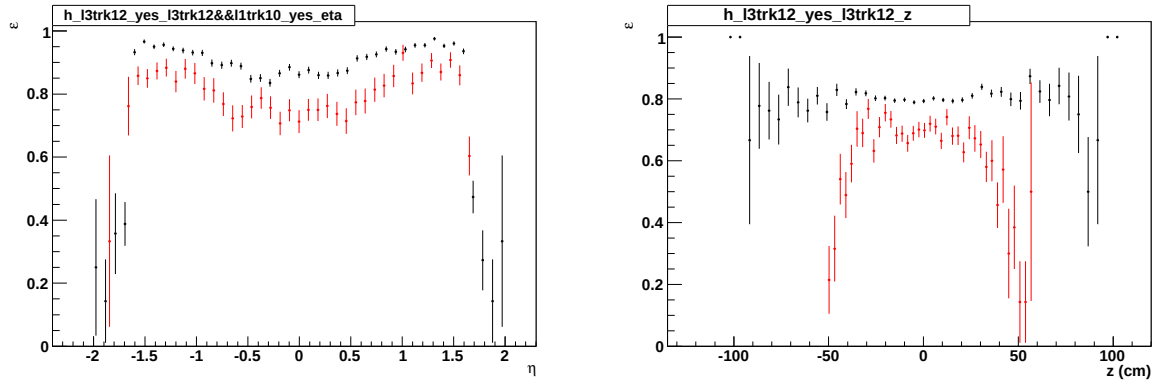

Figure 50: *The dependence of the Level 3 Track, $p_T > 12$ GeV term, on CFT detector eta and z, relative to loose offline tracks that have fired the level 1 track, $p_T > 10$ GeV term for data taken before triggerlist v14 (black) and data taken with triggerlist v14 (red).*

7.3 LeveL-3 muon central matching

7.4 Di-muon trigger

Di-muon triggers are combinations of single muon trigger objects. Their efficiencies can be obtained by multiplying the efficiencies for single-muon objects if it assumed that single object efficiencies are uncorrelated.

This assumption is not valid if the muons are not well separated muons ($\Delta R > xx$ no study have been conducted to define what is x yet. 0.5 seems a rather safe minimum separation). A correlation also arises from the back to back octant boundaries. quantitative statements to be done.

8 Muon Backgrounds

In this section, we outline the common backgrounds in muon analysis, and the cuts which can be used to reject them. The backgrounds considered are:

- Muons from cosmic rays (section 8.1)
- Muons from in-flight decay (section 8.2)
- Fake muons from punch-through (section 8.3).

Other analysis-specific backgrounds (such as semi-leptonic quark decay backgrounds to $W \rightarrow \mu\nu$) are not covered here.

8.1 Muons from Cosmic Rays

Muons from cosmic rays passing through the detector can be reconstructed as back to back, opposite charge muons. In the case that the muon is only reconstructed entering or leaving the detector, a cosmic muon can appear as a a single muon event. To reject cosmic muons, cuts on muon scintillator hit time, track dca, and acolinearity between central tracks can be used. In the case of single muon events, a veto on the presence of another muon roughly back to back with the selected muon can also be used. The veto may use looser quality cuts - e.g. not requiring a track match to the second muon, or rejecting loose rather than medium muons. This should be studied before use in analysis.

8.1.1 Timing Cuts

As the arrival of cosmics is uncorrelated with a $p\bar{p}$ collision, they typically produce 'out of time' hits. Muons from collisions produce hit times close to zero, so cosmics can be rejected by (when information available):

- |A-layer time| < 10 ns
- |B-layer time| < 10 ns
- |C-layer time| < 10 ns

These cuts are implemented in the isCosmic() flag in MuoCandidate.

Cuts on scintillator times alone do not reject all cosmics - the scintillator trigger gates to preferentially select cosmic muons which have hit times close to zero, reducing the effectiveness of this cut.

However, in the case of dimuon events, a cut on the time difference between the A-layer hits on each muon (Δt_A) is very effective against cosmics. Typically, it takes a cosmic monn around 20 ns to cross the distance between the A-layer on one side of the detector and the A-layer on the other side (around 6 m), so requiring $\Delta t_A < 12$ ns rejects most of these.

8.1.2 dca Cuts

When a muons is matched to a central track, a cut on the track dca is very effective against cosmics, as they are not constrained pass through the beam position in x-y. In the case of fairly 'empty' events (such as $Z \rightarrow \mu^+\mu^-$or $W \rightarrow \mu\nu$), using the track dca to the beam spot is recommended[2]. For higher occupancy events (e.g. muon plus jets), the primary vertex is more reliable and can be used.

A loose cut would be to require the muon track to have a dca < 0.2 cm. Tighter cuts would be dca < 0.02 cm for tracks with SMT, dca < 0.2 cm for tracks without SMT hits.

When using the primary vertex, requiring a match between the vertex and the muon track in z of around 3 cm is also an effective cut.

The timing cuts with a cut of dca < 0.2 cm is implemented in the isCosmicTight() flag in MuoCandidate. Unfortunatly in p17, this dca is computed relative to (0,0), so that the isCosmicTight flag is sensitive to the beam displacement. So it should be considered that this flag is bugged and it is recommanded not to use it.

8.1.3 Acolinearity Cuts

Acolinearity (really, this is pseudo-acolinearity), A, which can be used in di-muon events, where both muons are track-matched. Acolinearity between the two muon tracks is defined as:

$$A = \pi - |\Delta\phi| + |\Sigma\theta - \pi|, \tag{4}$$

where $\Delta\phi$ and $\Sigma\theta$ are the angles between the two tracks. Cosmic muons pass straight through the detector, producing back-to-back tracks with small acolinearity. Requiring $A > 0.05$ rejects most cosmics.

In the case of single muon events, acolinearity can still be used, but must be applied with more care. Here, a cut can be placed on the acolinearity between the muon track and any other track with comparable curvature and matching z in the event. However, this method is more likely to also reject signal events in which another track happens to be back to back with the muon, and should be studied before use.

8.2 Muons from In-flight Decays

Note that the studies in this part has been done on p14 data. However it is thought they are still relevant for people analyzing p17 data.

Another source of real muons is from pion and kaon decays. Pions and kaons that decay inside the tracking volume (extending to a radius of 52 cm) produce 'kinked' tracks which can be reconstructed as high pT, and this has been found to be a significant background in high pT single muon analyses. Decays outside the tracking volume do not affect the tracking, but have not so far been found to be a problem in analysis. Also, this background has not been found to be a problem in di-muon analyses, with the probability of two in-flight decays in one event being negligible.

The symptoms of this background are:

[2]The beam spot is produced by the AATrack algorithm, and is stored in the beamspot-2.09 file available in the head version of this package

- A poorly reconstructed central track, either with high χ^2/d.o.f. or missing hits (or both), caused by the kink at the decay point.
- Tracks containing a kink generally have poor momentum and *dca* resolution, as they are a mixture of the hits caused by the pion/kaon and muon.
- The resulting muon will be of lower momentum than the initial pion / kaon. Combined with the effects of poor track resolution, this leads to a large discrepancy between the central track momentum, and the momentum measure in the muon system.

This background is most visible in the local muon pT distribution, and can be removed using cuts on the fit χ^2/dof and dca of the central track. As an example, figure 51 shows the local pT from the W $\rightarrow \mu\nu$ cross section analysis. Here, a medium muon with a matched central track with pT > 20 GeV and SMT hits. The local pT distribution before and after applying cuts on the χ^2/dof and dca of the central track show the presence of in-flight decay in the low local pT region. It can be seen that the χ^2/dof cut is most effective, but with the combination of this and the dca cut it is possible to almost entirely eliminate this background. Typical cuts are to require $\chi^2/dof < 3.3 - 4$ and dca $< 0.011 - 0.02$ cm for tracks with SMT hits, and dca < 0.2 cm for tracks without SMT hits. This background is larger for muons without SMT hits.

A cut of local pt $> 10 - 14$ GeV would also remove in-flight decays. However, this will also remove many signal muons in the overlap region (around $\eta = 1$), where the local momentum resolution is poor (these muons produce the low local pT peak visible in figure 51 after applying the χ^2/dof and dca cuts).

8.2.1 In-flight Decays in Monte Carlo

A problem was found in the Monte Carlo for pion and kaon decays. In cases where the pion or kaon decayed outside a radius of 52 cm (the radius of the central tracker), the resulting muon was not being added to the MC truth table. In future releases, all muons from pion/kaon decay will be added to the truth table (note: muons resulting from showering will not be added).

8.3 Fake muons from punch-through

Again a p14 result.

In some cases, particles from a high energy jet can leak out of the calorimeter and produce hits in the muon system. This produces a source of fake non-isolated muons. Generally, these fake muons appear as A-segments, but the definition of 'medium' muon quality allows A-segments matched to central tracks in the bottom region of the detector. So, when looking at non-isolated muons, it is recommended to use 'medium + nseg$>$ 1' requirements. This ensures hits before and after the toroid, and eliminates most of this background. Figure 52 shows the distribution of medium muons in jets before and after requiring a BC hit on the muon. This plot is taken from D0 Note xxxx.

Another feature observed in non-isolated muons is the muon 'horns'. This is an excess of muons around $|\eta| = 1$, which roughly corresponds to the overlap between the central and forward muon system. Figure 53 shows a typical distribution.

This does not seem to be caused by duplicate muons - the horns are observed even in a sample of single muon events. However,in this region there is less material between the

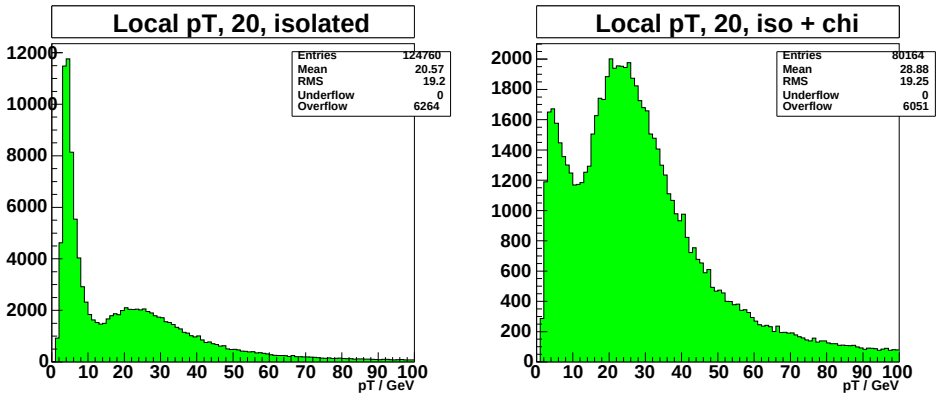

(a)

(b)

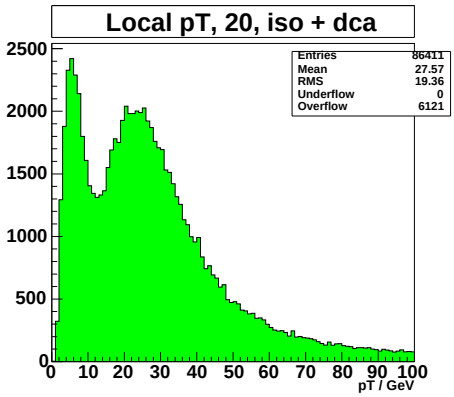

(c)

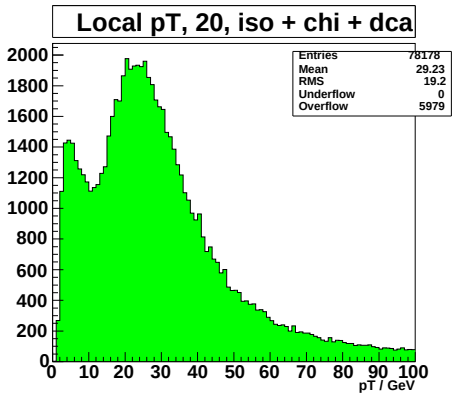

(d)

Figure 51: Histogram showing the local momentum of muons in the W $\rightarrow \mu\nu$ cross section analysis (a) before applying the χ^2/d.o.f. and dca cuts, (b) after applying only the χ^2/d.o.f. cut, (c) after applying only the dca cut amd (d) after applying both cuts.

interaction and muon system, so it may be easier for lower pT muons (and other particles) to reach the muon system and be reconstructed. However, at the moment there is no definite explanation for the horns.

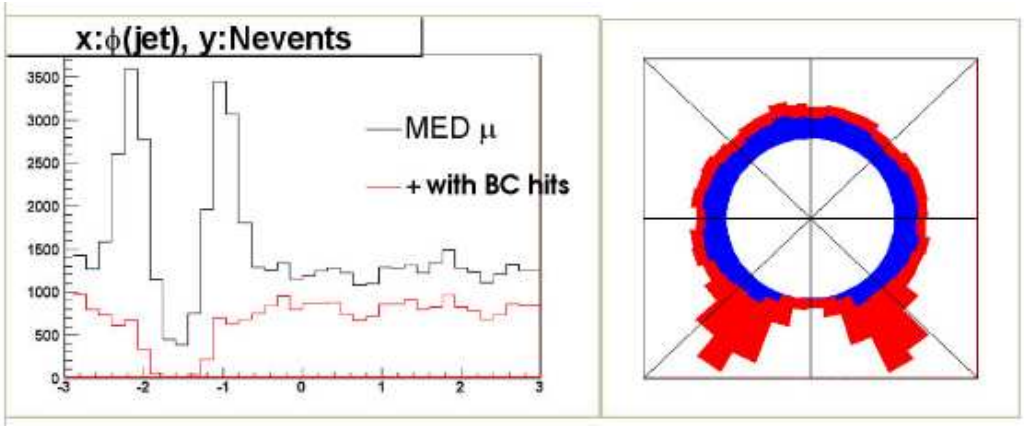

Figure 52: Punch-through, seen with teh standard definition od 'medium' muons, and reduced by requiring BC hits.

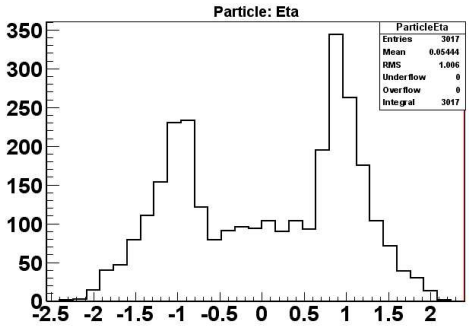

Figure 53: The muon 'horns', visible in a sample of non-isolated muons.

9 Momentum Resolution and MC smearing

In this part the momentum resolution in Data and MC are presented and the smearing of the MC momenta necessary to have similar resolution in data and MC is described.

9.1 Method

The resolution is estimated from the width (and shape) of the Z^0 peak. In fitting the measured Z^0 peak and interpreting the fit results several of effects have to be considered.

- The width and shape of the peak is due to the convolution of the genuine Drell-Yan spectrum and the muon resolution.
- The quantity which contributes with a Gaussian resolution is not the invariant mass but $1/p_t$ of the two muons.
- Both muons may have different resolutions. This is especially the case if both muons have different track qualities (e.g. one is without SMT hits.)

In order to take these effects into account the measured the Z peak is fitted by a convolution of the parton level Drell-Yan spectrum and a Gaussian function in $1/M$.

$$f(M) = \int DY(m) p_0 e^{-0.5[1/M - 1/(m-p_1)]^2/p_2^2} (\frac{m-p_1}{M})^2 dm$$

The parameters p_0, p_1, and p_2 denote the normalization, a shift of the peak, and the width of a Gaussian resolution in $1/M$. The term $(\frac{m-p_1}{M})^2$ is due to the fact that $1/M$ instead of M is assumed to have a Gaussian resolution. The parton level Drell-Yan spectrum $DY(m)$ is taken from the Monte Carlo truth information. Fig. 54 shows that the fit is able to describe the data much better than a fit which assumes a Gaussian resolution in M. It is also important to note that the fit does not require an additional background contribution.

In order to test the method true $1/p_t$ was smeared with a Gaussian before calculating the invariant mass. The fits are shown in Fig. 55. Both in the case that the two muons were smeared with the same width and with different width, the assumed fit function is able to describe the distribution and p_2 is given by:

$$p_2 \times 91\text{GeV} \approx \frac{\sigma(1/M)}{1/M} = 0.5 \sqrt{(\frac{\sigma(1/p_T^{\mu 1})}{1/p_T^{\mu 1}})^2 + (\frac{\sigma(1/p_T^{\mu 2})}{1/p_T^{\mu 2}})^2}$$

In the case that $1/p_T$ of both muons is smeared by 0.1/40GeV one gets a value of $p_2 \times 91\text{GeV} = 0.074$ compared to the expectation of 0.071 if all muons have $p_T = 40\text{GeV}$ and the dimuon mass is 91GeV. If only one muon is smeared one obtains $p_2 \times 91\text{GeV} = 0.052$ compared to the expectation of 0.050. The muon momentum resolution and the MC smearing are determined by either smearing the Monte Carlo truth or the full simulation as function of p_t, η and track quality by the amount necessary to simultaneously produce distributions with the same width in data and MC for the different combinations of possible muon chooses (e.g. both muons with SMT hits and $|\eta_{\text{CFT}}| < 1.6$, one muon with $|\eta_{\text{CFT}}| > 1.6$ one muon without SMT hits).

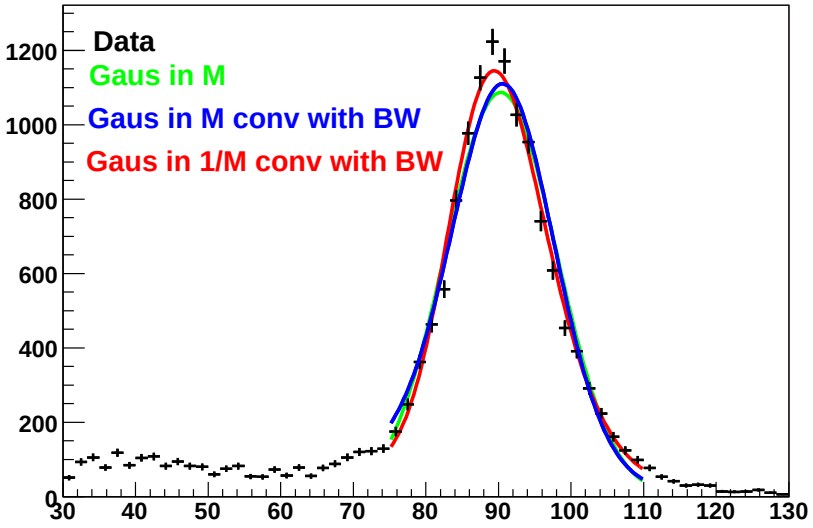

Figure 54: *Fit of the Drell-Yan spectrum with different fit functions.*

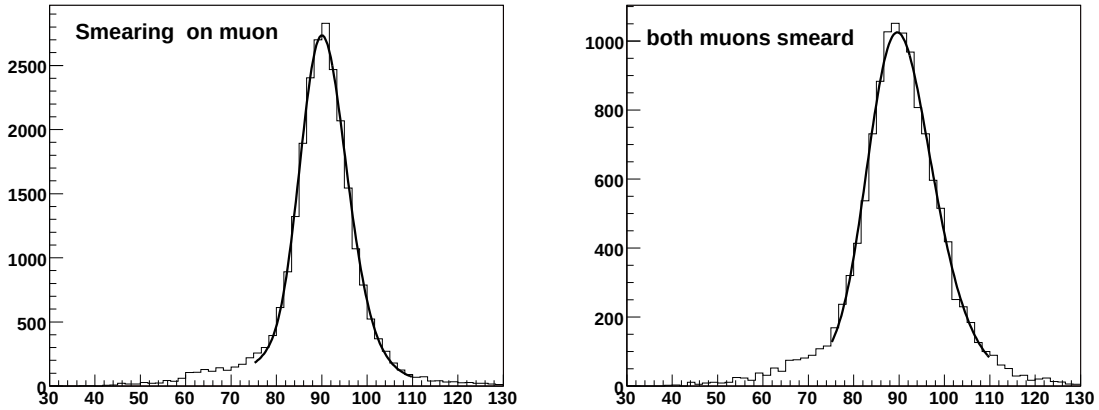

Figure 55: *Fit of the the dimuon mass calculated form the smeared Monte Carlo truth information. Either for both or only for one muon* $1/p_T$ *was smeared by* $0.1/(40\text{GeV})$.

In order to study the p_T dependence, samples where either both muons have $p_T > 40$GeV or both muons have $p_T < 40$GeV were used. The kinematic bias of this selection on the dimuon mass was included into the fit function by an additional correction factor calculated as the ratio of the dimuon mass with and without the additional p_T cut using smeared Monte Carlo events. The fits to the data for both cases are shown in Fig. 56. Again one gets a good description.

In order to determine the smearing parameters the values of the fit parameters are only indirectly used. The Monte Carlo is smeared to give the same fit results as the data. Therefore it is only important that the fit gives a good description of the data. However the fact that the

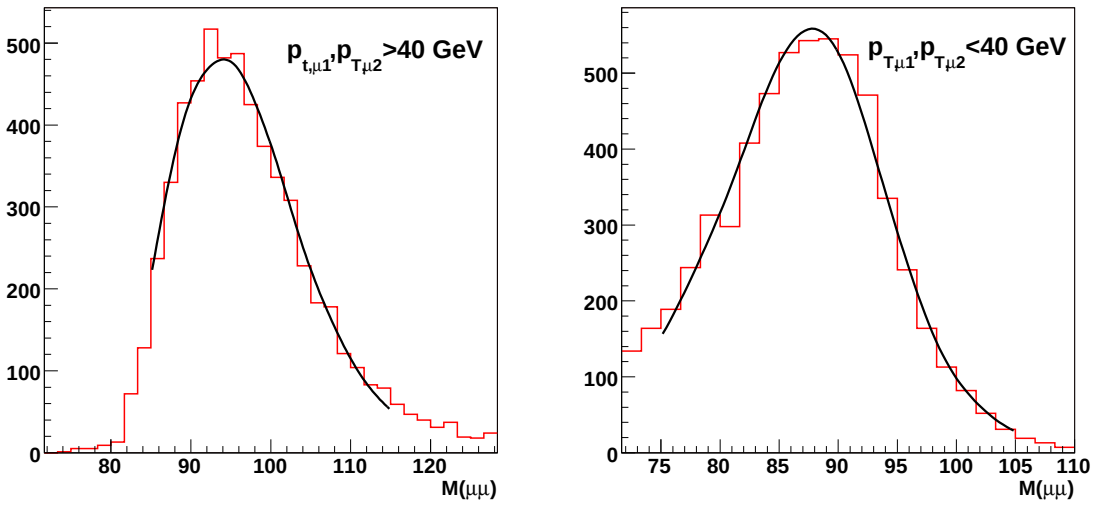

Figure 56: *Fit of the the dimuon mass for data events where either both muons have* $p_T >$ 40GeV *or* $p_T <$ (40GeV).

fitted width and shift of the peak position have the expected values give additional confidence in the ansatz.

9.2 Monte Carlo Smearing

The smearing parameters are determined for a smearing of either the form:

$$\frac{q}{p_t} \rightarrow \frac{q}{p_t} + (A + B_1/p_T) \times \text{Rnd}$$

or:

$$\frac{q}{p_t} \rightarrow \frac{q}{p_t} + (A + B_2 \times p_T) \times \text{Rnd}$$

Where Rnd is a Gaussian (width 1, center 0) distributed random number. The momentum range of muons from Z^0 decays is not large resulting in a relatively large uncertainty of the p_T dependence. The fit is therefore preformed in two stages. The complete sample is used to determine the smearing at $p_T = 40$GeV, which corresponds to the average muon p_T in the sample, by fitting $A_0 = A + B_1/40\text{GeV}$ or $A_0 = A + B_2 \times 40\text{GeV}$ while fixing the ratio $R = B/A$. Samples where either both muons have $p_T > 40$GeV or both muons have $p_T < 40$GeV where used to determine the ratio $R = B/A$. In order to avoid a possible dependence on the result for A_0 from the initial selection of R the process was iterated. The resolution is separately determined for three types of muons.

- Muons with SMT hits and $|\eta_{\text{CFT}}| < 1.6$
- Muons with SMT hits and $|\eta_{\text{CFT}}| > 1.6$

- Muons without SMT hits.

η_{CFT} is the detector η in the CFT-detector and is therefore a measure for the number of possible CFT-hits a track could have. For $|\eta_{\mathrm{CFT}}| > 1.6$ tracks do not any more pass all CFT layers. The parameters are determent by requiring that the fit of the Drell-Yan spectrum as described in section 9.1 returns the same width in data and the smeared Monte Carlo simultaneously in three samples.

- Both muons have SMT hits and $|\eta_{\mathrm{CFT}}| < 1.6$.
- Both muons have SMT hits. At least one muon has $|\eta_{\mathrm{CFT}}| > 1.6$.
- One muon has SMT hits, the second one has no SMT hits.

For muons without SMT hit the momentum is recalculated from the error matrix imposing the constraint that it originates from the run average beam spot. The run average beam spot is used instead of the primary event vertex because the later is not necessary well measured in events only containing two muons, one without SMT hits. The data statistic are not large enough to study samples where both muons have $|\eta_{\mathrm{CFT}}| > 1.6$ or have no SMT hits. Therefore the samples listed above are selected, this however leads to correlations between the resolutions. The resolution for muons with SMT hits and $|\eta_{\mathrm{CFT}}| < 1.6$ is determined by the first sample. Most events in the second sample however still contain one muon with $|\eta_{\mathrm{CFT}}| < 1.6$. Therefore the estimated resolution of muons with $|\eta_{\mathrm{CFT}}| > 1.6$ will depend on that of muons with $|\eta_{\mathrm{CFT}}| < 1.6$

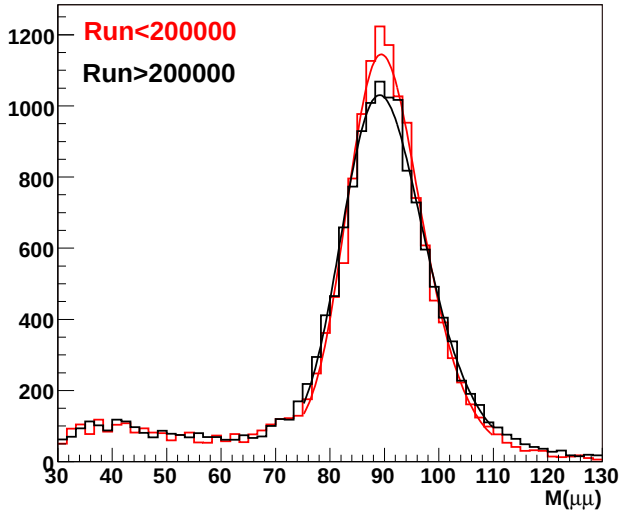

Figure 57: *Comparison of the resolution for pre- (run number $< 2 \cdot 10^5$) and post-shutdown data (run number $> 2 \cdot 10^5$)*

The resolution drastically changed between data taken in runs before the fall 2004 shutdown (run number $< 2 \cdot 10^5$) and data taken after the shutdown. This is shown in Fig. 57. Smearing parameters and resolutions are therefore determined separately for the two data periods.

Fig. 58, 59, and 60 show the comparison between the pre-shutdown data and the smeared Monte Carlo. One can see that the smeared MC and the data agree within the statistical uncertainty of the data. The smearing parameters are listed in Table 6.

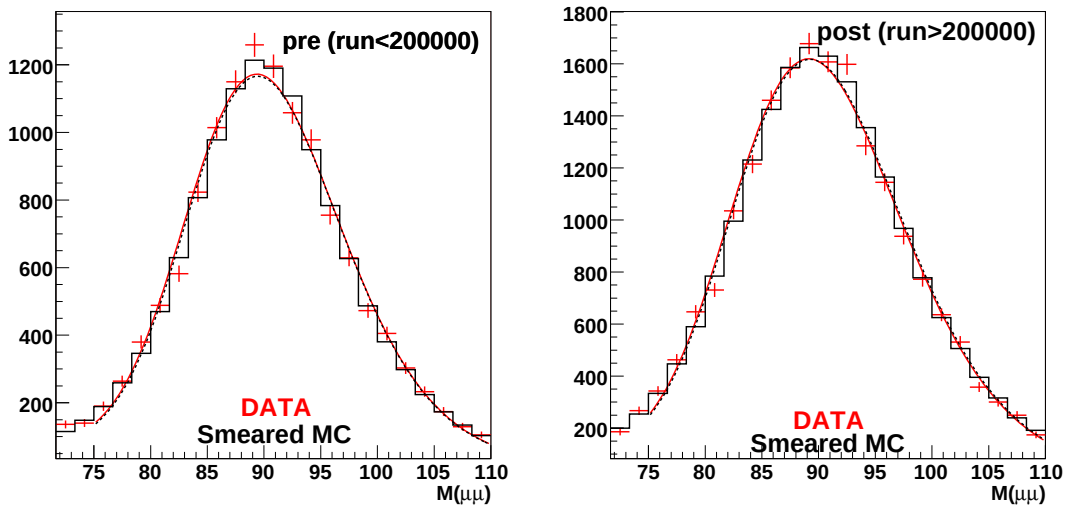

Figure 58: *Comparison of data and smeared Monte Carlo for events where both muons have SMT hits and* $|\eta_{\rm CFT}| < 1.6$. *(The MC sample only contain events with parton level masses* > 60 *GeV.)*

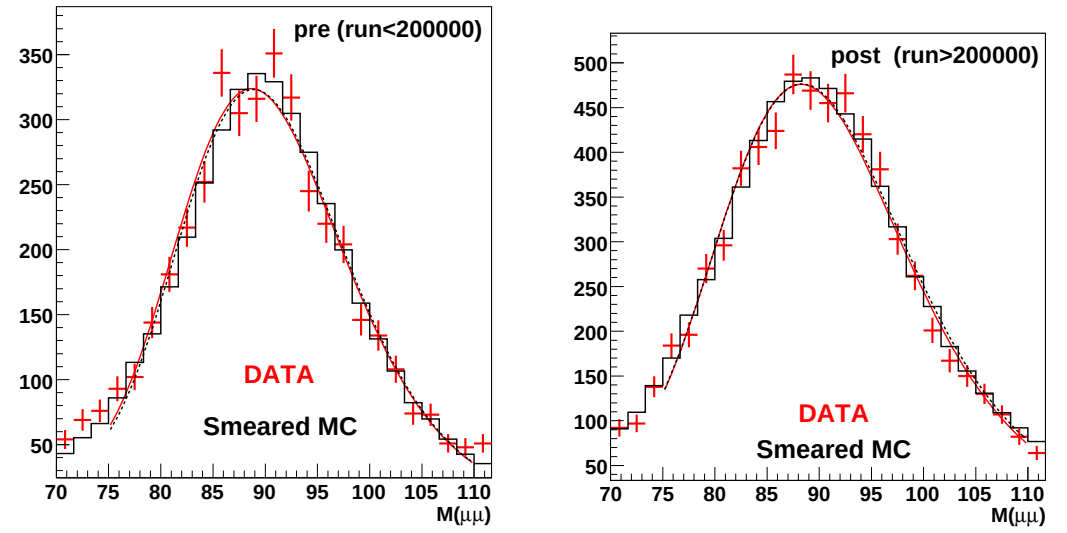

Figure 59: *Comparison of data and smeared Monte Carlo for events where both muons have SMT hits and one muon has* $|\eta_{\rm CFT}| > 1.6$. *(The MC sample only contain events with parton level masses* > 60 *GeV.)*

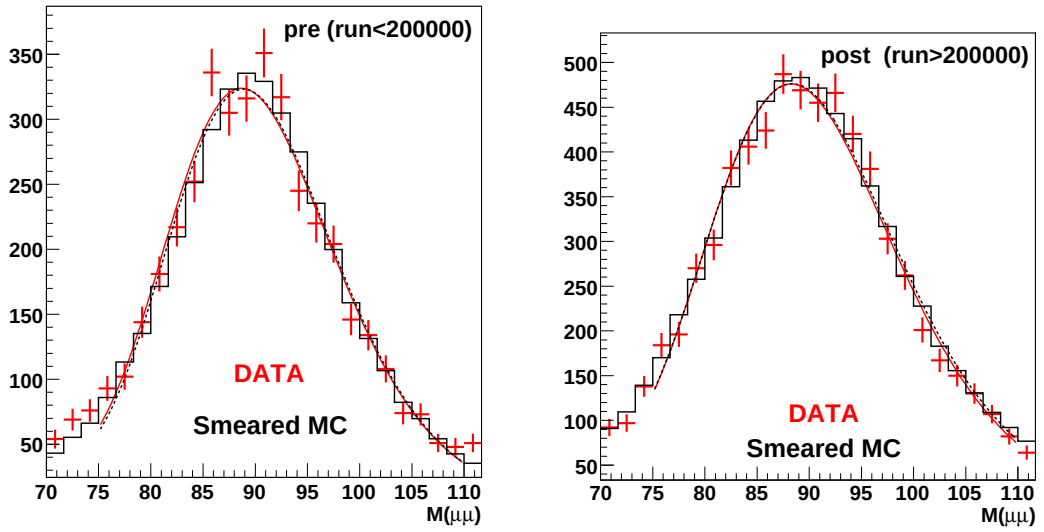

Figure 60: *Comparison of data and smeared Monte Carlo for events where one muon has SMT hits and the other muon has no SMT hits. (The MC sample only contain events with parton level masses* > 60 *GeV.)*

	run $< 2 \cdot 10^5$		run $> 2 \cdot 10^5$	
	A	B_1	A	B_1
SMT hits $\eta_{\mathrm{CFT}}\| < 1.6$	0.00313	-0.0563	0.00308	-0.0370
SMT hits $\eta_{\mathrm{CFT}}\| > 1.6$	0.00273	-0.0491	0.00458	-0.0550
no SMT	0.00509	-0.0916	0.00424	-0.0509

Table 6: *Default smearing parameters for the parametrization* $A + B_1/p_T$

In addition to the width of the Z^0 peak the fit also returns the peak position. A possible difference in the position between data and Monte Carlo could be interpreted as a different momentum scale in data and Monte Carlo, which could be corrected with an additional scaling of the Monte Carlo momenta. The results for the comparison yield a scaling factor for the muon p_T of $S = 0.9995 \pm 0.0010$ for the pre- and $S = 0.9990 \pm 0.0012$ for the post-shutdown data. ($1/p_T$ would have to be scaled by $1/S$.) The quoted errors are due to the variation of the p_T dependence of the smearing and the statistical uncertainty of the peak position in the data. The later contributes 0.0006 to the error. The factors are consistent with 1, therefore no scaling is implemented in the standard smearing.

9.3 Monte Carlo Smearing uncertainties

In addition to the default smearing parameters additional parameter sets have be generated corresponding to the statistical uncertainties and the difference between using track quality "none" and "medium". For the first two sets the ratio $R = B_1/A$ was fixed to the central value. They therfore represent the uncertainties on $A_0 = A + B_1/40\mathrm{GeV}$ (the average smearing). The

two sets are compared in Fig 61 with the data. The two bars for the data show the difference between using track quality "none" and track quality "medium". One can see that the -1σ Monte Carlo is below the data in the tails of distribution whereas the $+1\sigma$ Monte Carlo is above in the data peak region.

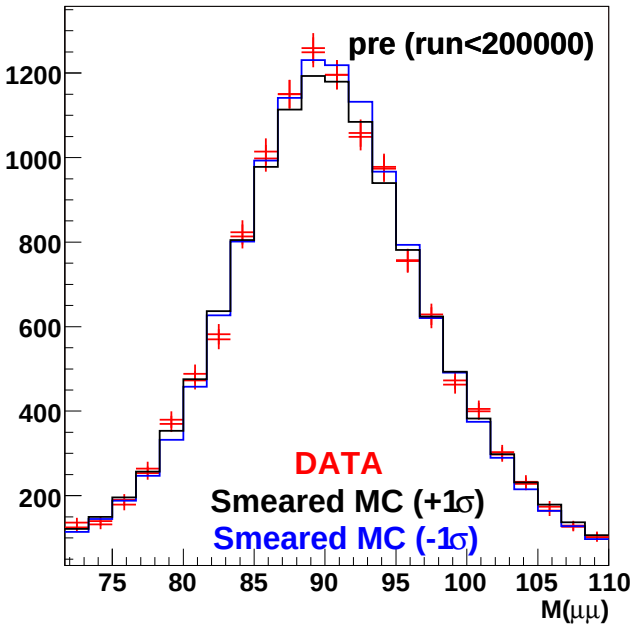

Figure 61: *Comparison of pre-shutdown data and smeared Monte Carlo for events where both muons have SMT hits and* $|\eta_{\mathrm{CFT}}| < 1.6$. *The two Monte Carlo distributions represent the* $\pm 1\sigma$ *variation of the average smearing. The two data error bars represent the different track quality (medium and none).*

Two more parameter sets where calculated to estimate the uncertainties of the p_T dependence for a fixed average smearing (A_0) at the central value. All five parameter sets where both calculated for the parametrization $A + B_1/p_T$ and $A + B_2 \times p_T$. The uncertainty of the p_T dependence for muons with $|\eta_{\mathrm{CFT}}| > 1.6$ or without SMT hits are very large. Especially for the case of a stronger p_T dependence the parametrization was bounded by $B_1/(40\mathrm{GeV})/A < -1$ and $B_2/A < \infty$. Fig. 62 shows the p_T dependent smearing $A + B_1/p_T$ or $A + B_2 \times p_T$ for the different parameter sets. The p_T dependence is estimated from muons which still have p_T relatively close to 40GeV. The extrapolation to large and small p_T is therefore strongly dependent on the selected parametrization. For $p_T < 30\mathrm{GeV}$ and $p_T > 60\mathrm{GeV}$ the difference between the two parameterizations get significant. In this range no reliable prediction of the smearing using only Z^0 events is possible.

9.4 Resolution

The muon resolution in data can be determined in two ways. In an approach followed by the top group [15] the smeared reconstructed muon p_T is compared in Monte Carlo events with the

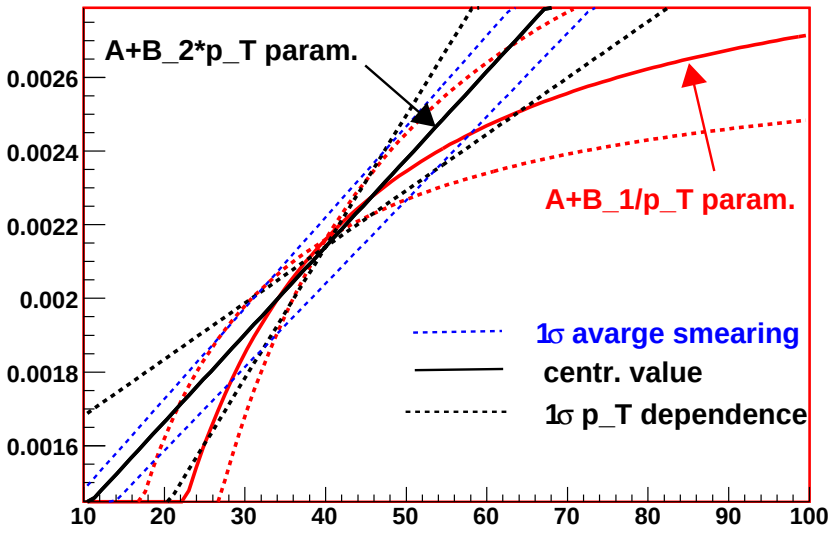

Figure 62: *Smearing paramter as function of p_T for events where both muons have SMT hits and $|\eta_{\mathrm{CFT}}| < 1.6$. The dashed line indicate the one σ uncertainties of the two parameterizations.*

true parton level muon p_T. In this approach all effect which are well described in the Monte Carlo (e.g. the number of CFT hits as function of η_{CFT}) can be estimated with high statistical precision. One has however to be aware that the estimate is based on the Monte Carlo smearing described above and has therefore the same statistical and systematic limitations. A more direct approach is the smearing of the Monte Carlo truth instead of the reconstructed Monte Carlo p_T. In this ansatz the smearing can be directly interpreted as resolution. For muons with with SMT hits and with $\eta_{\mathrm{CFT}} < 1.6$ On gets a smearing parameters of $A_0 = A + B_1/(40\mathrm{GeV}) = 0.00240 \pm 0.00008$ ($A_0 = A + B_1/(40\mathrm{GeV}) = 0.00275 \pm 0.00008$) for the pre- (post-) shutdown data. For a $p_T = 40\mathrm{GeV}$ muon with SMT hits and with $\eta_{\mathrm{CFT}} < 1.6$ this results in a resolution of $\delta p_T/p_T = 9.6 \pm 0.3\%$ for the pre-shutdown and of $\delta p_T/p_T = 11.0 \pm 0.3\%$ for the post-shotdown data.

References

[1] http://www-d0.fnal.gov/computing/algorithms/muon/muon_algo.html

[2] Gavin Hesketh for the D0 Muon Algorithm and Identification groups, *Content of the p17 Muon Thumbnail*, D0note 4735

[3] http://www-d0.fnal.gov/Run2Physics/working_group/data_format/caf/classTMBMuon.html

[4] wzreco and muo_cert documents:
https://plone4.fnal.gov/P1/D0Wiki/mu_id/muo_cert/
http://www-d0.fnal.gov/d0dist/dist/releases/development/wzreco/doc
http://www-d0.fnal.gov/d0dist/dist/releases/development/muo_cert/doc
D0 note in preparation

[5] Common Sample Group web: http://www-d0.fnal.gov/Run2Physics/cs/index.html

[6] Common Analysis Format web: page http://www-d0.fnal.gov/Run2Physics/cs/caf/

[7] muid_eff package to compute and store muon related efficiencies:
https://plone4.fnal.gov/P1/D0Wiki/mu_id/muid_eff/

[8] ApplyMuonSmear documentation:
http://www-d0.fnal.gov/d0dist/dist/releases/development/caf_util/doc/html/classcaf__util_1_1ApplyMuonSmear.html see also TMBMuon documentation http://www-d0.fnal.gov/Run2Physics/working_group/data_format/caf/classTMBMuon.html

[9] MuonSelector documentation:
http://www-d0.fnal.gov/d0dist/dist/releases/development/caf_util/doc/html/classcaf__util_1_1MuonSelector.html

[10] Documentation for correcting the MC efficiencies within CAF:
http://www-d0.fnal.gov/d0dist/dist/releases/development/caf_eff_utils/doc/html/

[11] Documentation for computation of trigger efficiencies within CAF:
http://www-d0.fnal.gov/d0dist/dist/releases/development/caf_trigger/doc/readme.html

[12] Emily Nurse and Paul Telford, DØ Note 4689, 'Measurement of the Cross section for Inclusive Z Production in Di-muon Final States at $\sqrt{s} = 1.96$ TeV'.

[13] F. Déliot, G Hesketh, P Telford, B Tuchming, DØ Note 4749, 'Measurement of $\sigma(p\bar{p} \to WX) \times \mathrm{Br}(\mathrm{W} \to \mu\nu)$ at $\sqrt{s} = 1.96$ TeV'

[14] Heidi Schellman, DØ Note 5142, 'The longitudinal shape of the luminous region at DØ'

[15] Petra Haefner and Frank Fiedler , DØ Note 4818 'Determination of the Muon Transfer Function for Top Mass Measurements', DØ Note 5214, 'Muon transfer function parameters for p17 MC'.